Characterization of Reactive Dissolution and Swelling of Polymer Films Using a Quartz Crystal Microbalance and Visible and Infrared Reflectance Spectroscopy

W. Hinsberg,* F. A. Houle, S.-W. Lee, and H. Ito

IBM Research Division, Almaden Research Center, San Jose, California 95120

K. Kanazawa

Department of Chemical Engineering, Stanford University, Stanford, California 94305

Received June 21, 2004; Revised Manuscript Received December 17, 2004

ABSTRACT: Dissolution and swelling of thin films of ionizable polymers in contact with aqueous alkaline solutions are examined using a quartz crystal microbalance, while simultaneously recording the visible reflectivity and infrared absorption of the evolving films. From these data changes in the thickness, depth structure, composition, mass, and mechanical properties of the polymer film during its interaction with the aqueous solution can be detected. Analysis of these provides evidence for the formation of interfacial gel layers resulting from acid−base reaction of the polymer with the hydroxide solution and yields information on the kinetics of transport and chemical reaction that control the overall process. Kinetics simulations indicate that the most important factors influencing observed behaviors are the intrinsic reactivity of ionizable groups on the polymer and the response of the film's mechanical properties, which determine the ability of small molecules to move through it, to incorporation of water.

Introduction

A significant body of work has examined experimental and theoretical characteristics of swelling[1−5] and dissolution[6−10] of glassy polymer films by organic solvents. These are purely *physical* processes and differ from the *reactive* dissolution and swelling of polymer films in contact with an aqueous solution, where typically an acid−base reaction alters the polymer structure and thereby its solubility properties. Reactive dissolution and swelling are by nature more complex since the kinetics of the chemical reaction influence the observed dissolution behavior. Reactive swelling and dissolution of drug/polymer composites are used for the controlled release of therapeutic agents in biological systems, and there have been numerous studies of their function in that context.[11] Reactive dissolution also serves as the foundation for imaging of all modern polymeric photoresist materials.[12] Here a radiation-induced patternwise chemical modification of a thin polymeric film alters its dissolution properties such that exposed and unexposed regions can be differentiated when immersed in an appropriate developer solution. This application of reactive dissolution provides the context for the present work.

Reactive Dissolution in Resist Materials

Phenolic polymers (for example, *m*-cresol novolacs and poly(4-hydroxystyrene) derivatives) have been used extensively in photoresists intended for patterning using ultraviolet light of wavelengths of 248 nm and greater.[12] The weakly acidic phenolic hydroxyl group serves as a site for ionization and solubilization of the chains by a developer solution containing aqueous hydroxide ion. Experimental studies of the reactive dissolution of such polymers have been confined in large part to the analysis and interpretation of bulk dissolution rates as a function of polymer properties or composition of the aqueous solution.[13−17] This is due in part to the long-held view of reactive dissolution as a surface-limited process more closely akin to the acid-mediated etching of metals or the dissolution of quartz by hydrofluoric acid than to polymer dissolution by an organic solvent. The presence of an interfacial transition layer during phenolic polymer dissolution has been proposed,[18−20] and though experimental results have been interpreted as being consistent with that,[18,19] the behavior of such materials is viewed by some to remain an open question.

Recently, the pursuit of photoresist materials optimized for imaging with 193 and 157 nm excimer laser exposure sources has led to evaluation of nonaromatic polymer systems with ionizable functionality, for example, carboxylic acids and fluorinated alcohols.[21,22] These groups are alternatives to phenolic repeat units, which are too optically opaque at these wavelengths for practical use. In studies using quartz crystal microbalance[23] (QCM) dissolution rate monitors, several such polymer systems were shown to exhibit anomalous QCM frequency changes when immersed in aqueous base solutions, behavior consistent with significant permeation of the liquid developer components into the film (leading to swelling) prior to dissolution.[24,25]

We report here experiments that characterize the response of thin films of polymers bearing base-reactive groups when immersed in aqueous alkaline solutions. The specific systems chosen for study probe a progression of behaviors: (i) water permeation, (ii) permeation of aqueous base accompanied by significant swelling but no dissolution, (iii) aqueous base dissolution of a polymer mediated by a thick gel layer, and (iv) aqueous base dissolution of a polymer mediated by a thin-to-nonexistent gel layer. In chemical terms, they span kinetics in which the relative rates of base transport, polymer reaction, and polymer transfer into the liquid phase are each varied, enabling the signatures of each stage of the dissolution process to be evaluated experimentally. Time evolution of each film is recorded using a QCM dissolu-

10.1021/ma048772t CCC: $30.25
Published on Web 02/08/2005

tion monitor, with simultaneous high-speed visible reflectance interferometry or infrared reflectance spectroscopy. The QCM, specifically designed to measure frequency and resistance shifts in the compound oscillator, responds to changes in film mass and film mechanical properties stemming from its interaction with the solution. Reflectance interferometry yields detailed information on the evolving physical structure of the film, and infrared spectroscopy provides complementary data about accompanying chemical changes. Reaction−diffusion kinetics simulations allow a unified picture of the essential chemistry and physics to be developed. They show that the apparently disparate behaviors observed for different materials can be understood simply in terms of the interplay between transport and reaction in each type of polymer.

Principles of Analytical Methods

QCM Frequency-Resistance Analysis. In a QCM, a piezoelectric quartz crystal is configured as the frequency-determining component of an electronic oscillator circuit, and changes in its oscillation frequency are recorded. Mass uptake or removal at the electrode surface is reflected by a change in the oscillation frequency. For a thin, rigid film applied to the crystal surface, the frequency shift is linear with the mass of the applied film, a relation first expressed by Sauerbrey:[26]

$$\Delta F = -\frac{2F_0^{\,2}}{\sqrt{\rho_Q \mu_Q}} m' \qquad \text{(I)}$$

where F_0 is the resonant frequency of the unloaded resonator, m' is the mass density of the film, ρ_Q is the density of the quartz crystal, and μ_Q is its shear modulus corrected for piezoelectric stiffening. In our initial application of a QCM to the characterization of dissolution kinetics,[23,27] eq I was shown to apply when measuring the dissolution of glassy polymer films, a typical example being a photoresist based on diazonaphthoquinone−novolac chemistry. In general, though, an applied viscoelastic film will influence the resonance behavior of the loaded quartz crystal in a more complex fashion.

Impedance analysis of the quartz resonator can provide additional information on the solid/liquid interface.[28−30] The well-established Butterworth−van Dyke (B−VD) equivalent circuit provides a framework for relating electrical properties of the quartz oscillator to mechanical properties of deposited films.[31] Among the B−VD circuit elements, the motional resistance represents energy loss due to damping and is closely related to the physical properties of any deposited films and adjacent liquid.[31,32] When combined with a quantitative model for the compound resonator structure, changes in that resistance can provide an assessment of the properties of the applied film.[33] In the present work, a compensated phase-locked oscillator (CPLO) driver circuit[34] facilitates direct measurement of both the resonance frequency and motional resistance at high data rates that provide millisecond time resolution.

Visible Reflectance Interferometry. The visible reflectivity of smooth, thin transparent films is dominated by optical interference.[35] The absolute reflectance R is determined by materials optical properties (the wavelength-dependent complex refractive indices of the incident medium, the film, and the substrate and the film thickness) and by the polarization, angle of incidence, and wavelength of the interrogating light beam. Film structural details can be inferred by fitting multiwavelength reflectance spectra to those predicted by well-established thin film optical models.[36] Multiwavelength techniques have been applied previously to the characterization of resist dissolution,[37,38] but in those cases the acquired data were not well-suited for comparison to theoretical values.

Figure 1 demonstrates how structure and optical properties of a polymer film layer influence reflectivity. Figure 1a displays visible reflectance spectra calculated[36] for the surface-limited etch-type dissolution of a polymer film with a refractive index of ∼1.6 applied to a silicon wafer. A small change in film thickness leads to significant change in its reflectance spectrum. This family of curves highlights a useful property: for a uniform material, the extrema of its reflectance spectra will always fall along two curves (shown as dotted lines on each graph), determined by the optical constants of the incident medium, the substrate, and the thin film.[35] If during dissolution the optical properties of a film change homogeneously, for example due to rapid uniform infusion of a solvent of lower refractive index throughout the film, this would be signaled by an upward vertical shift of the minima from the theoretical limit (Figure 1b) while the maxima remain without offset. In a third hypothetical case a 45 nm surface layer containing equal volume fractions of polymer and solvent forms at the liquid−film interface due to permeation of solvent in the initial stages of dissolution. Such an interfacial layer has a refractive index intermediate between solvent and polymer and therefore functions as an antireflection coating[39] whose quantitative impact on reflectance depends on its solvent volume fraction and thickness. The overall result is both an upward shift in the spectral minima *and* a downward shift in the spectral maxima (Figure 1c).

In the present work, multiwavelength reflectance spectra of the polymer film spanning the visible wavelength region are recorded simultaneously with the frequency and resistance of the quartz oscillator and using a common time base. This facilitates direct comparison of film structure derived from reflectance analysis with the measured changes in film mass and mechanical properties that the QCM analysis provides.

Infrared Reflectance Spectroscopy. Infrared (IR) spectroscopy is widely applied to compositional analysis. In this work we use an IR reflectance spectrometer microscope to record sequential spectra of polymer thin films on metal-coated piezoelectric quartz wafers immersed in aqueous alkaline solution, concurrent with QCM analysis. In conventional aqueous solutions, strong water absorption obscures spectral regions of interest in the IR region, so in these experiments solutions of hydroxide ion in deuterated water (D_2O) are used, shifting interfering absorptions to lower frequencies.

Experimental Section

Materials. Figure 2 depicts the chemical structures of the polymers examined in this study.

Poly(norbornene ethyl carbonate-co-norbornene carboxylic acid) (P(NBCarb-NBCA)). This material, a copolymer of 5-(ethoxycarbonyloxy)methyl-2-norbornene (NBCarb) and bicyclo[2.2.1]hept-2-ene-5-carboxylic acid (NBCA), was obtained from B.F. Goodrich Co. (now Promerus Electronic Materials, Brecksville, Ohio) as a solid and was used as 12−15 wt % solutions in propylene glycol monomethyl ether

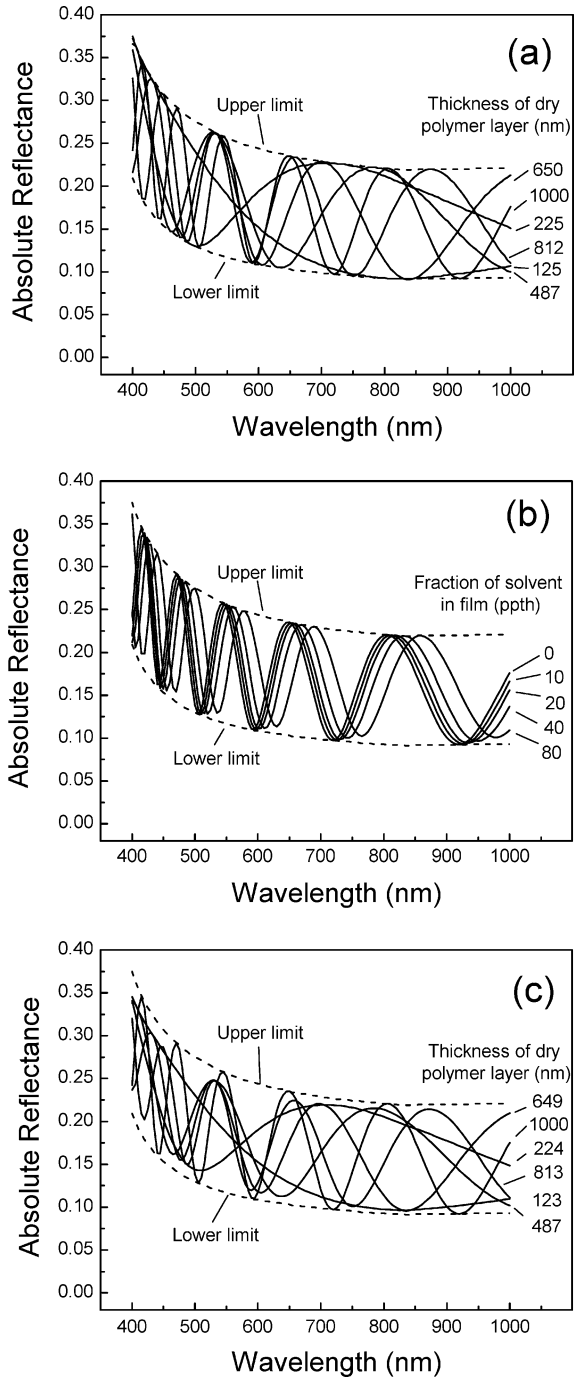

Figure 1. Model calculations for the visible reflectance of 1000 nm thick polymer film on silicon immersed in a liquid: (a) for dissolution assuming surface limited etching and no permeation of the liquid into the film; (b) for swelling of the film by uniform permeation of the film by the liquid; (c) for formation of an interfacial gel layer 45 nm thick, followed by dissolution of the film. In these calculations, the optical properties the liquid and the polymer film were set to those of water and a typical *m*-cresol novolac polymer, respectively.

acetate (PGMEA) casting solvent. The copolymer composition was 30 mol % norbornene carboxylic acid and 70 mol % of the norbornene carbonate ester. The polymer has a molecular weight M_w of 57 400 and a polydispersity of 1.8 as determined by gel permeation chromatography (GPC).

Poly(methyl methacrylate-co-methacrylic acid) (P(MMA–MAA)). This material was synthesized by conventional radical polymerization of methyl methacrylate and methacrylic acid in refluxing tetrahydrofuran solvent using 2,2′-azobis(isobutyronitrile) as the initiator.[40] The polymer molecular weight

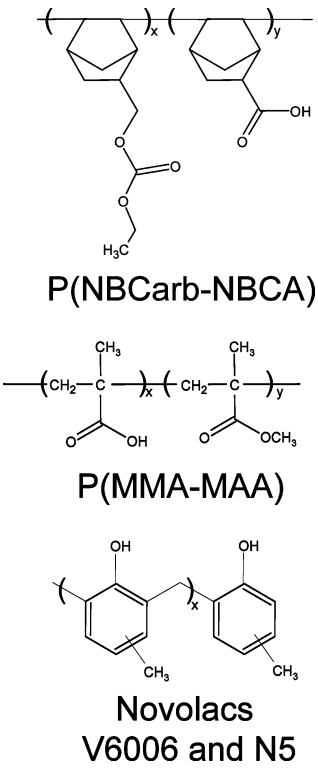

Figure 2. Chemical structures of the three polymers examined in this work.

M_w was 12 800 with a polydispersity of 1.83. Analysis of the polymer composition[41] by C-13 NMR showed that 18–21% of the polymer repeat units were methacrylic acid on a molar basis.

Cresol Novolacs (V6006 and N5). Varcum novolac resin lot V6006 (supplied by Varcum Chemical Co., now Durez Corp., Dallas, TX) is the product of polymerization of cresylic acid (a mixture of cresol isomers) with formaldehyde. V6006 has a M_w of 10 200 and a polydispersity of 8.5 as measured by GPC. The novolac resin lot N5 is prepared by polymerization of *m*-cresol with formaldehyde and is supplied by Eastman Kodak (Rochester, NY). GPC analysis of N5 shows a multimodal molecular weight distribution with peaks centered at 1790 and 4580 Da. These two polymers were coated from filtered solutions in diglyme (ethylene glycol dimethyl ether), using solution compositions of 26 wt % (V6006) and 30 wt % (N5) polymer.

Developer Solutions. Tetramethylammonium hydroxide (TMAH) solutions of varying normality were prepared by diluting Microposit CD-26 developer (a 0.26 N solution of TMAH in water, supplied by Rohm and Haas Microelectronics, Marlborough, MA) with appropriate volumes of deionized water. TMAH solutions in D_2O were prepared by dissolving TMAH pentahydrate (Eastman Kodak, Rochester, NY) in 99.9% deuterium oxide (Sigma-Aldrich, St. Louis, MO).

Instrumentation. Piezoelectric quartz sensor crystal substrates (part no. SC-501-1) were obtained from Maxtek, Inc. (Santa Fe Springs, CA). These substrates as received are patterned with gold electrodes and were used in that configuration for simultaneous reflectance IR spectroscopy/QCM analyses. The active area of the crystal, defined by the electrode pattern, is 6 mm in diameter and centered on the substrate. For visible reflectance/QCM measurements, the crystals were overcoated with 90 nm of chromium using an in-house vacuum evaporator. The reflectivity of the chromium overlayer is well-suited for optical reflectance in the visible spectrum. Optical constants (n and k vs wavelength) of the chrome-coated substrates in the visible spectrum were measured using a Woollam model M2000V spectroscopic ellipsometer (J.A. Woollam Inc., Lincoln, NE). The optical constants of all polymer films were obtained on 25 mm diameter silicon wafers using the same instrument.

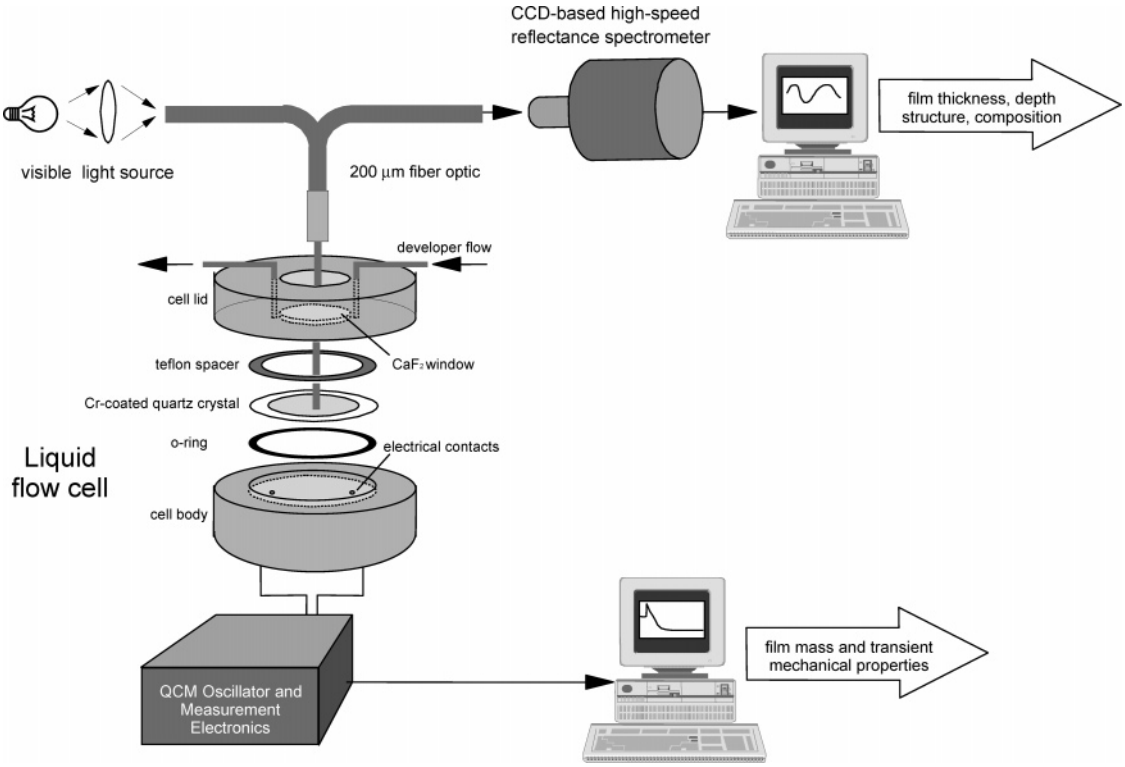

Figure 3. Schematic diagram of the combined reflectance spectrometer−QCM instrument.

Thin polymer films were formed by spin-coating and post-apply baking using a model 100CB spinner/hot plate (Cost-Effective Equipment Inc., Rolla, MO). The physical thickness of films was measured with using an Alpha-Step model 200 profilometer (Tencor Instruments, San Jose, CA) with an estimated precision of 50 nm.

Quartz Crystal Microbalance. The film-coated quartz resonator was mounted in a Maxtek CHK-100 crystal holder equipped with a Maxtek model FC-550 flow cell lid that had been modified by the addition of a transparent calcium fluoride window. The window allows viewing of the central portion of the coated substrate throughout the experiment. A Teflon spacer (using a thickness of 0.05 or 0.12 mm for infrared or visible reflectance, respectively) between the crystal and the cell lid defines the volume of the flow cell (10 and 24 μL, respectively). Figure 3 shows an exploded view of the flow cell. Liquid is delivered to the flow cell under computer control using a model KDS200 syringe pump (KD Scientific, New Hope, PA). After filling the syringe, the inlet tubing is purged with the liquid until all air bubbles are eliminated.

The crystal oscillation is driven by a compensated phase-locked oscillator (CPLO) circuit[34] that produces a dc voltage output proportional to the admittance of the liquid/film/crystal compound resonator and an ac signal oscillating at the undistorted resonant frequency of the circuit. That frequency is measured using a Fluke model 6681/016 high-resolution timer−counter operating in high-resolution externally gated mode connected to a PC through a GPIB connection. The value of the admittance signal is measured using the A−D converter on board either an ATMIO-16E-10 or a PCI 6023E data acquisition card (both supplied by National Instruments, Austin, TX). The data acquisition card is configured to generate periodic trigger signals that control the overall timing of data acquisition. The relationship between the CPLO output voltage and the true admittance of the resonator was established by immersing an uncoated oscillating crystal sequentially in a series of glycerol/water mixtures. For each mixture the change in admittance upon immersion was measured using a Hewlett-Packard model HPE5100A network analyzer and mode HP41941-61001 impedance probe, and the voltage shift in the admittance signal of the CPLO circuit was measured using the same crystal and liquid mixture.

Visible Reflectance Spectrometer. The visible reflectance instrumentation used in this work is shown schematically in Figure 3. Emission from a model LS-1 incandescent light source (Ocean Optics Inc., Dunedin, FL) is focused into one arm of an Ocean Optics model R200-7 bifurcated fiber optic. The probe end of the fiber optic is a 200 μm diameter fiber bundle that directs the light through the calcium fluoride window of the flow cell and the flowing liquid onto the polymer-coated QCM crystal at normal incidence. The light reflected normal to the film reenters the fiber optic and is spectrally analyzed using an Ocean Optics model PC2000 spectrometer configured for the spectral region from 360 to 1000 nm. Custom in-house software is used to control calibration, data acquisition, and analysis. Each time an external trigger signal is received, a full spectrum is recorded using a 3 ms integration time. The spectral region between 450 and 850 nm, containing measured reflectance values at approximately 400 different wavelengths, is saved for later analysis. This range corresponds to that where the overall spectrometer signal is most strong. The final data are presented and analyzed in the form of absolute reflectance vs wavelength. The instrument is capable of recording up to 100 full spectra per second. For simultaneous QCM−reflectance analyses, the same trigger signal controls QCM data acquisition.

Infrared Spectrometer. Infrared spectra were acquired using Nicolet Continuum infrared microscope (Thermo-Nicolet, Madison, WI) configured for reflectance measurements and attached to a Nicolet Nexus 470 Fourier transform infrared spectrometer. To record IR spectra simultaneously with QCM measurements, the spectrometer was operated in rapid scan series mode, acquiring one spectrum per second with 16 scans per spectrum.

Methods. *Dissolution Measurement.* The procedure for a typical dissolution experiment is as follows. Prior to coating, a spectrum (IR or visible reflectance) of the blank substrate mounted in the liquid-filled cell is recorded for calibration. For the visible reflectance measurement, both flat field (with the illumination source transmitting light through the optical system) and dark field (with the illumination source blocked) spectra are recorded. The crystal is then rinsed with deionized water and dried, and the polymer film is applied by spin-coating from a filtered solution of the polymer. This is

immediately followed by a post-apply bake (at 130 °C for 60 s except for the novolac polymers which were post-apply baked at 120 °C for 60 s). After coating, the crystal is placed in the dry flow cell which is then reassembled. Under computer control, QCM and reflectance data acquisition are initiated at a predetermined data rate, and the fluid flow through the cell is then started, at a flow rate of 5.0 mL/min unless otherwise stated. Data acquisition is continued for a predetermined time at which time the liquid flow is stopped and the data are saved.

Visible Reflectance Data Analysis. The visible reflectance spectrometer outputs a series of spectra containing raw reflected light intensity expressed in arbitrary units as a function of wavelength. Each raw spectrum is converted into an absolute reflectance spectrum by applying scaling corrections for the lamp spectral output, spectrometer wavelength response and dark signal, and window losses. These correction factors are calculated from the flat field and dark field spectra acquired as part of each dissolution measurement. In some cases a final small scaling correction to account for differences in positioning of the substrate between mountings is applied.

Analysis of the resulting set of absolute reflectance spectra was carried out by chi-square fitting to those predicted for a multilayer thin-film optical model. The optical model defines the liquid developer layer as the incident medium and the chromium-coated substrate as the emergent medium. The developing/swelling polymer layer is represented by the model in a flexible and configurable way so the absolute reflectance of a range of differing film structures can be predicted and compared to experiment. The polymer layer can be configured to be a single layer of constant or variable composition and thickness or can be partitioned into a two-layered structure where a dry, glassy layer in contact with the substrate is topped by an interfacial layer whose refractive indices are intermediate between those of the liquid and the dry polymer layer. The boundary separating the two layers can be specified to be sharp or diffuse with a finite width. The composition and thickness of each layer can be independently designated to be variable or to have a fixed value.

Quantitative predictions of film reflectance spectra were calculated using an in-house implementation of the Berning and Berning algorithms.[35] A fitting procedure based on the Levenberg−Marquardt method[42] adjusts those parameters designated by the user as variable to provide a best fit between the experimental spectra and those predicted for the optical model. Each spectrum in a time series was analyzed independently using as initial values for the variable parameters the final values from fitting of the spectrum immediately preceding it in time. For the first spectrum in a time series, the initial value for the polymer film thickness was estimated by evaluating the wavelength positions of spectral maxima and minima.[43]

Estimation of Mechanical Properties. We have reported an extension of the physical model for the quartz resonator[28] to include the case where two viscoelastic layers are deposited on the resonator immersed in a liquid.[33] This model allows the prediction of resistance and frequency shifts, given the density and viscosity of the liquid, and the thickness, density, viscosity, and elastic modulus of each layer. Each QCM−reflectance experiment provides resistance shift and film thickness vs time. From these data a table of resistance shifts as a function of layer thickness can be constructed. By fitting resistance shift vs thickness curves predicted by the physical model with these data sets (again using the Levenberg−Marquardt method for chi-square analysis), estimates for the elastic modulus and viscosities of the lossy (energy-dissipating) interfacial layer can be obtained. For reference the resistance shifts of the insoluble polymers poly(styrene), poly(ethyl acrylate), and poly(butyl acrylate) were evaluated by spin-coating films on QCM substrates at varying thicknesses, baking to remove residual coating solvent, immersing the coated crystal in deionized water, and calculating the resistance shift due to the film by subtracting the resistance of the immersed uncoated crystal.

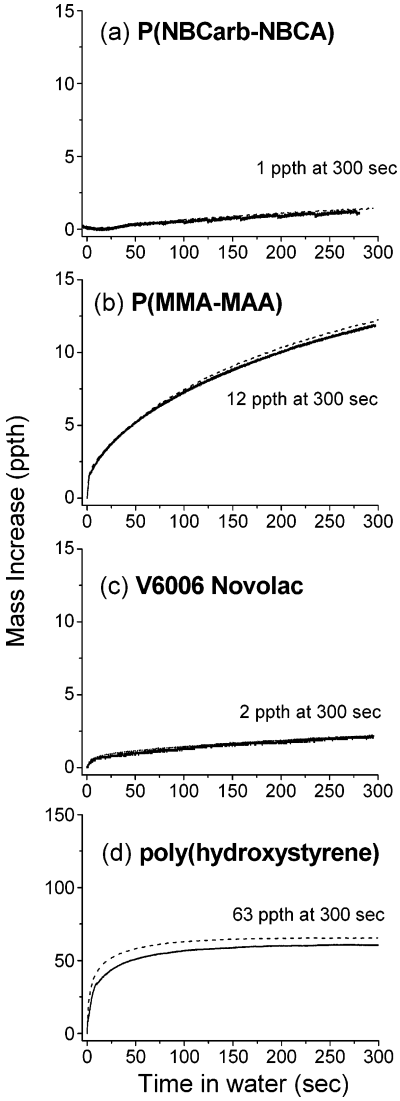

Figure 4. Mass increase due to water permeation into 1 μm thick films of P(NBCarb-NBCA), P(MMA−MAA), novolac V6006, and poly(hydroxystyrene). Both the mass increase calculated from QCM frequency shift using the Sauerbrey equation (solid lines) and that calculated from the film thickness increase measured by optical reflectance (dashed lines) are shown and give consistent results. These data were obtained using a static liquid layer (no flow). Note the change in vertical scale for graph (d).

Results and Discussion

Permeation of Polymer Films by Water. An initial evaluation of polymer film permeability to deionized water free of added base is presented in Figure 4. Over a 300 s period (the maximum time scale of the dissolution experiments that follow) these films absorb between 1 and 12 parts per thousand (ppth) of water. In each case the change in film refractive index due to water uptake is sufficiently small (on the order of 0.2% or less) that no offset of minima or maxima in the reflectance spectra from those of the initial dry polymer is evident. Changes in film structure and composition when contacted with water are very small compared to those that occur when these films are immersed in aqueous hydroxide solutions.

For comparison, the water uptake of a poly(4-hydroxystyrene) (PHOST) film (M_w 35 600, supplied by Hoechst-Celanese, Somerville, NJ) is shown in Figure 4d. PHOST absorbs ~6 wt % water, consistent with

values measured by other techniques.[44,45] This is 30 times the water uptake of V6006 novolac over the same time period. We speculate that novolac exhibits decreased water absorption compared to PHOST due to a difference in intramolecular hydrogen bonding, in analogy to its effect on dissolution.[46] Measurements of water absorption by very thick, vacuum-dried films of formulated diazonaphthoquinone−novolac resist show substantially greater water uptake,[47,48] but differences in film composition, thickness, and experimental methodology make direct comparison with the present results impractical.

Base-Induced Swelling in P(NBCarb-NBCA). *Visible Reflectance Spectrometry.* The cyclo-olefin polymer P(NBCarb-NBCA) presents a range of behavior when contacted with aqueous base, from extreme swelling to rapid dissolution depending on the ratio of comonomers.[25] Here, the copolymer containing 30 mol % of the carboxylic acid monomer NBCA was selected for study, a composition that swells extensively but does not dissolve appreciably under our conditions. Figure 5a displays reflectance spectra recorded as a film of P(NBCarb-NBCA), initially 1090 nm thick as coated, swells in contact with a 0.066 N solution of TMAH. These spectra exhibit complex changes in the amplitude, positions, and number of extrema, diagnostic of changes in film structure as developer permeates the film. This time series of reflectance spectra can be analyzed using the four-layer optical model, assuming in addition to liquid and substrate layers the presence of a "dry" layer (i.e., not permeated by developer) and a developer-swollen layer, separated by a well-defined, abrupt boundary. Composition and thickness of the gel layer and the thickness of the dry layer were designated as variable and independent fitting parameters. Calculated reflectance curves using best-fit values for the dry layer thickness and the gel layer thickness and composition at each point in time are overlaid with the experimental curves in Figure 5a. Figure 5b plots best-fit values for gel layer thickness, composition, and dry layer thickness vs time that result from this reflectance analysis. The rate of increase of the gel layer and the rate of decrease of the dry layer are strictly linear with time. The composition of the gel layer averages about 55 vol % liquid during this stage. The thickness of the gel layer reaches a plateau after the dry layer has been completely consumed; a slow secondary swelling process follows.

For several polymers that exhibit physical swelling, the widths and concentration profiles of the moving front separating swollen and unswollen regions have been experimentally characterized.[2,4,5,49] In general, those results depict relatively sharp fronts, consistent with case II type transport.[50] The form of the front (its width and composition profile) influences reflectivity of the overall film structure in a specific way.[4] That characteristic can be used to estimate for the P(NBCarb-NBCA) system a front width by systematically examining how its value improves agreement between experimental and calculated spectra. Initial trials showed that for these data the analysis is insensitive to the precise form assumed for the composition profile across the front width (e.g., a linear vs a cosine vs an exponential gradient form), so for this purpose the front is described as a simple linear composition gradient of width w where liquid content ranges from that of the gel layer to zero liquid in the dry layer (Figure 6a). The full set

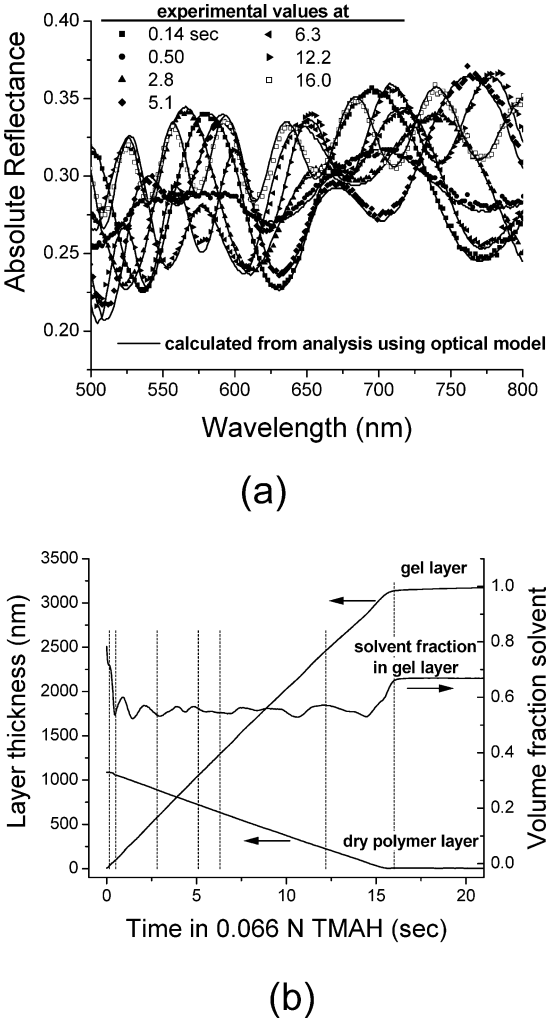

Figure 5. Visible reflectance analysis of the swelling of a film of P(NBCarb-NBCA). (a) Selected visible reflectance spectra recorded at different times during swelling. The discrete points represent the measured spectra, and the solid lines show those predicted from the optical analysis. Each reflectance spectrum contains values at 388 wavelengths between 500 and 800 nm (not all points are shown on the graph). (b) Thickness of the dry and swollen layers and solvent content of the swollen layer during swelling. Each of these curves is comprised of 30 data points per second of elapsed time. The vertical dashed lines indicate the times where the selected visible spectra shown in (a) were recorded.

of time series spectra were repeatedly fit to the four-layer optical model assuming different values for the front width w. Figure 6b plots the mean-square error (MSE), a measure of the goodness of fit between model and experiment, that results from these analyses. The fit between experiment and model is best (i.e., the MSE is minimized) when a front width in the range 5−50 nm is assumed.

Single-wavelength laser interferometry has been applied to study dissolution and swelling in polymer films.[4,5,19,38,51] To compare our results to these prior studies, plots of reflectance at a single wavelength in the visible spectrum can be extracted from the set of multiwavelength spectra. Figure 7 displays one such plot, in this case at 600 nm wavelength and assuming a value for w of 5 nm. The reflectivity undergoes a complex periodic variation, in line with similar reflectivity measurements reported for the swelling of poly(methyl methacrylate) (PMMA) in methanol.[4] There the appearance of high-frequency components in the reflec-

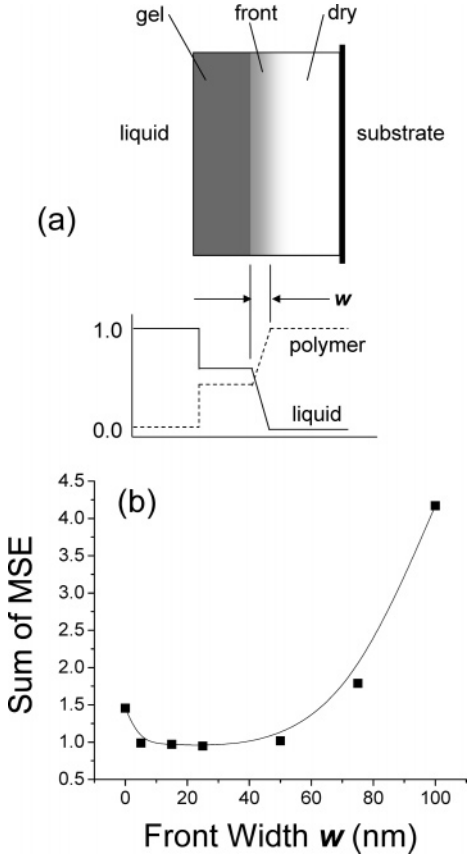

Figure 6. (a) Schematic of swelling polymer film showing the reaction front of width w and the polymer and liquid content of the various layers. (b) Plot of the mean-square error (MSE) from fitting a gel layer−dry layer optical model and experiment using different fixed values of the front width w. Each MSE was calculated by summing the individual chi-square values from fitting 450 individual reflectance spectra in the time series from 0 to 15 s.

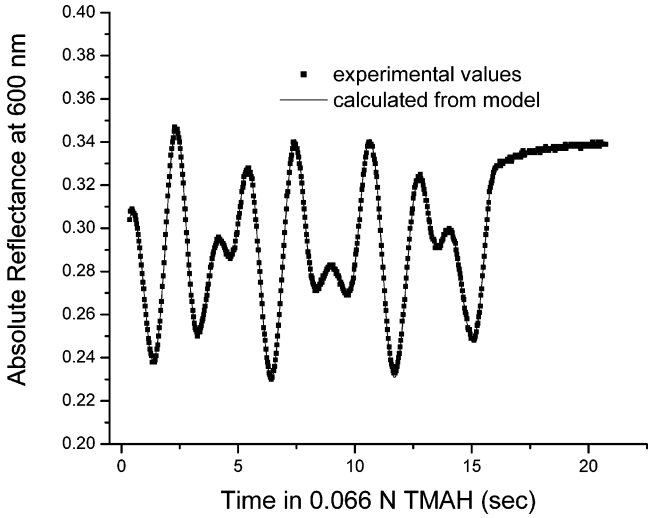

Figure 7. Reflectance at 600 nm wavelength of a P(NBCarb-NBCA) film undergoing swelling in contact with 0.066 N TMAH. Both the experimental reflectance and that calculated assuming a front width of 5 nm are shown.

tivity trace, observed at elevated temperatures in the PMMA/methanol case, was shown to be consistent with the presence of a sharp front with a width less than 0.2 λ (~120 nm in that case).

QCM Analysis. Since the densities of polymer and developer, the thickness of the dry layer and the

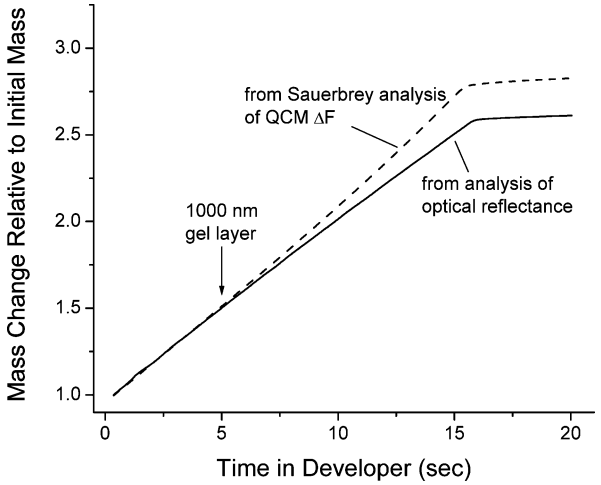

Figure 8. Comparison of mass change upon swelling of P(NBCarb-NBCA) in 0.066 N TMAH, as calculated from film optical reflectance and from QCM frequency shift.

thickness and composition of the gel layer are known for each point in time; these data can be used to calculate the mass change of the composite film as swelling occurs. Figure 8 compares the film mass vs time calculated from the reflectance analysis to that obtained by applying the Sauerbrey equation (eq I) to the frequency shifts from the QCM measurement performed simultaneously. Up to a total mass increase of ~50%, which corresponds to a gel layer thickness of ~1000 nm and a dry layer thickness of ~500 nm, the film mass calculated from the QCM frequency shift overlays that data. Beyond this the calculated masses diverge, with the Sauerbrey mass calculation giving a larger value than predicted from the optical analysis. The deviation is expected and is in accord with predictions of the extended QCM theory.[33] The resistance of the QCM oscillator shifts extensively as the polymer film swells and can be used to estimate the mechanical properties of the gel. This is addressed in later discussion.

IR Analysis. Acid−base neutralization chemistry plays a role in P(NBCarb-NBCA) swelling. As envisioned in this work, the neutralization reaction is a one-step description of a much more complex process in which a proton is transferred from the polymer to an OH^- accompanied by one or more waters of solvation, followed by relaxation of the spatial configuration of the anionic polymer and its surrounding water molecules to a local energy minimum. IR spectroscopy can be used to characterize the time evolution of that neutralization. Figure 9a plots shifts in QCM oscillation frequency and resistance that occur during swelling of P(NBCarb-NBCA) in contact with a 0.14 N solution of TMAH in D_2O. Film swelling is essentially complete at 35 s elapsed time. Figure 9b depicts changes in IR absorption that take place during this experiment. Initially an absorption at 1743 cm^{-1} is observed, attributed to the C=O bond stretches of the pendant carboxylic acid and carbonate ester groups. After swelling is complete, the carbonyl absorption has decreased and shifted, while a new absorption band centered at 1554 cm^{-1} has appeared. This new band can be assigned to the carboxylate ion formed by neutralization of the polymer's acid groups.[52]

Figure 9c plots the increase in the integrated area of the 1554 cm^{-1} carboxylate absorption over the same

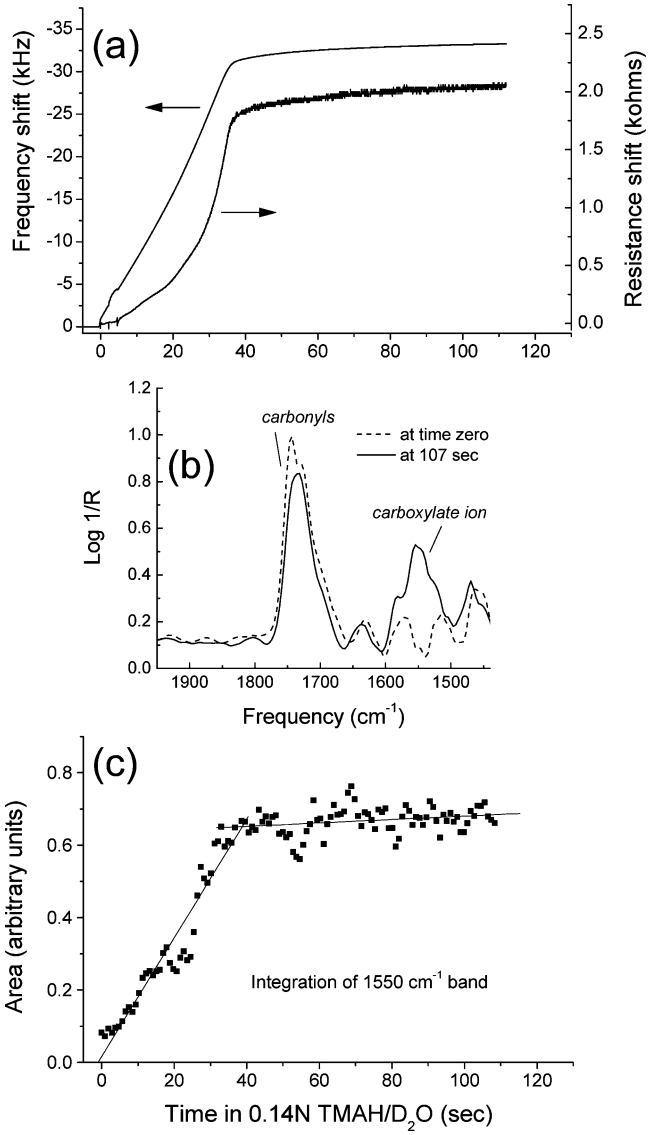

Figure 9. (a) Plot of the frequency shift and resistance shift as a function of time for a 3000 nm film of P(NBCarb-NBCA) immersed in a solution of 0.14 N TMAH in D_2O. (b) Changes in the IR spectra of during that experiment. (c) Change in the integrated area of the 1554 cm^{-1} absorption with time following initiation of liquid flow. The deviations from linear behavior in this plot are attributable to the contribution of thin film interference to the measured reflectivity. The periodic oscillation on the baseline in (b) is due to such interference.

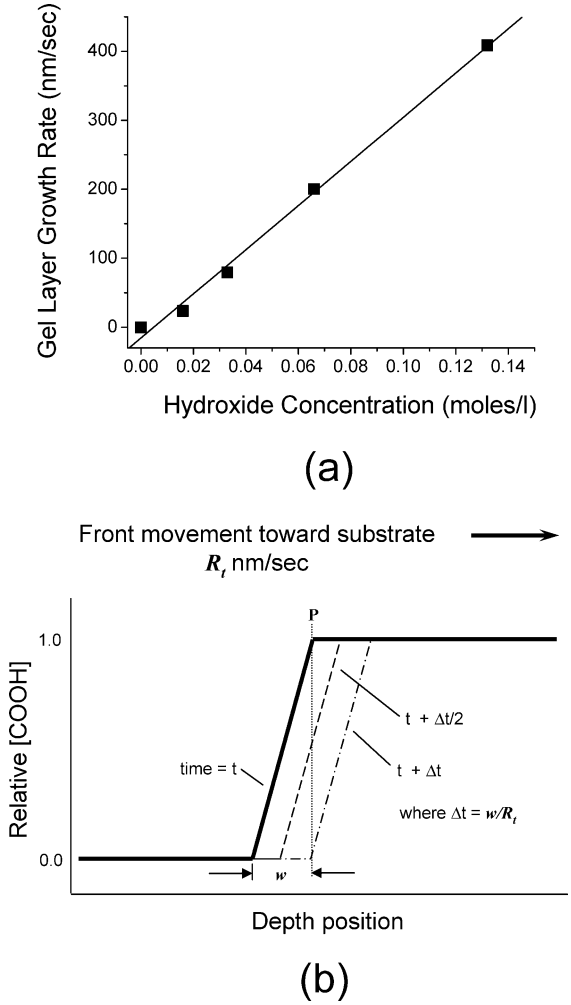

Figure 10. (a) Rate of gel growth in P(NBCarb-NBCA) measured by reflectance spectrometry, as a function of hydroxide concentration in the solution. At all concentrations examined, the gel thickness increases linearly with time. (b) Schematic diagram depicting the front separating gel and dry polymer layers in a swelling film of P(NBCarb-NBCA). The front is characterized by a gradient in chemical composition that advances through the film as swelling proceeds.

time scale as the QCM measurement. Changes in that absorption mirror those in the QCM data, exhibiting a sharp, essentially linear increase that plateaus when the dry polymer layer has been consumed. This correlation of IR and QCM time behavior is evidence directly linking swelling to conversion of the polymer from neutral to the more polar ionic form.

Effect of Hydroxide Concentration. Figure 10a plots the rate of gel growth of P(NBCarb-NBCA) as a function of liquid composition. The rate increases in direct proportion to hydroxide concentration. That observation, in combination with the IR analysis and the observation that the gel thickness increases linearly with time, is consistent with the following mechanistic picture. Neutralization of the polymer acid group by hydroxide that has permeated into the polymer is accompanied by immediate extensive hydration of the nascent solvated carboxylate anion. This acid−base reaction takes place in the region of the front separating dry and hydrated gel layers, and therefore it is in the region of the advancing front that hydroxide is consumed. The linear increase in the thickness of the swollen layer with time implies that the hydroxide concentration in the front region remains constant despite its increasing distance from the bulk solution. This in turn implies that the rate of hydroxide diffusion through the gel layer must be rapid compared to the rate of the neutralization reaction.

An averaged rate constant for acid−base neutralization during swelling of P(NBCarb-NBCA) can be estimated from these data. Consider a film of the polymer undergoing swelling in contact with a hydroxide solution of molar concentration C. At steady state the dry layer thickness decreases at a constant rate of $-R_t$ nm/s. Within the advancing front of width w nm, the extent of neutralization of the polymer acid groups varies (Figure 10b): at its leading edge acid−base neutralization has just begun while at its trailing edge neutralization has just reached completion. At a given position in the film depth (e.g., position P in Figure 10b) the polymer undergoes conversion from acid to carboxylate form when the front passes through that position in its

progression toward the substrate. If neutralization is the slow step in the overall swelling process, then the velocity of the front is proportional to the rate of the neutralization reaction; the time required for the front to move one front width toward the substrate (w/R_t) is equal to the time required for the COOH groups at position P to undergo complete neutralization. The neutralization rate at P can be described as

$$R_{\text{neut}} = \text{d[COOH]/d}t = -k_{\text{neut}}[\text{OH}^-][\text{COOH}] \qquad \text{(II)}$$

When the rate of transport of base to the front is large compared to rate of reaction, then [OH^-] will be constant, and the rate equation can be written as a pseudo-first-order reaction

$$R_{\text{neut}} = -k'_{\text{neut}}[\text{COOH}] \qquad \text{(III)}$$

where $k'_{\text{neut}} = k_{\text{neut}}[\text{OH}^-]$. If we choose the extent of reaction after five half-lives to represent complete neutralization, then

$$5t_{1/2} = w/R_t \qquad \text{(IV)}$$

from which estimates for k'_{neut} and k_{neut} can be calculated. Values for k_{neut} using the lower and upper limits estimated earlier for the front width w (5 and 50 nm), and assuming [OH^-] $\sim C$, are 750 and 75 L mol^{-1} s^{-1}, respectively. These values are 4−5 orders or magnitude below the limiting rate constant for a diffusion-controlled reaction estimated using the Smoluchowski equation,[53] assuming a diffusion coefficient for the base of 1×10^{-8} cm^2/s (a value typical for water diffusion in polymer films[54]) and a reaction cage radius of 1 nm. It should be emphasized that the neutralization reaction is more complex than the very simplified picture employed in this analysis. The front is not uniform in composition through its depth, and the rate constants derived here will average the effect on the neutralization rate of any compositional nonuniformity through the front.

Base-Induced Dissolution of P(MMA−MAA). Figure 11 plots the QCM resistance, and the film mass calculated from QCM frequency shift, during dissolution of P(MMA−MAA) for different solution concentrations of TMAH. Upon immersion the apparent film mass increases by 1−5%, and the resistance undergoes a significant upward shift. Following these initial increases, the mass decreases in a near-linear manner, while the resistance remains constant. At the end of the resistance plateau region, the resistance drops while the rate of mass loss increases by about 25%. Ultimately, both resistance and mass reach values for the uncoated crystal.

Mechanistically, the physical dissolution of polymers (for example, the dissolution of PMMA by an organic solvent) has been described as a three-stage sequence: (1) initial diffusion of solvent into the solid polymer matrix, leading to (2) solvation and swelling of the polymer network, which facilitates (3) the separation of polymer molecules from the network and diffusion into the bulk solvent.[55] Using this mechanistic framework, the QCM frequency and resistance changes shown in Figure 11 can be related to the evolving film structure as follows. Immediately following immersion, hydroxide ion and solvent diffuse into the rigid polymer matrix. Hydroxide−carboxylic acid neutralization creates ionic sites along the polymer chains that increase the polarity and hydrophilic character of the film in the interfacial region. As this proceeds, solvation of the ionic polymer by water leads to the formation of a developer-rich interfacial layer. The presence of solvent (along with the counterion) effectively plasticizes the film, leading to increased energy dissipation in the film due to viscous losses; this dissipation is signaled by an increase in resistance. The ionization and solvation proceed until the polymer chains at the interface are adequately ionized and are sufficiently mobile to dissolve into the solution. The thickness of the swollen interfacial layer remains constant during dissolution (as does its energy dissipation and therefore the resistance), which implies a steady state where the rates of developer penetration and separation of the ionized polymer from the swollen layer are equal. When the boundary of the interfacial layer with the solid polymer layer reaches the substrate, the magnitude of the resistance drops as the thickness of the swollen layer decreases.

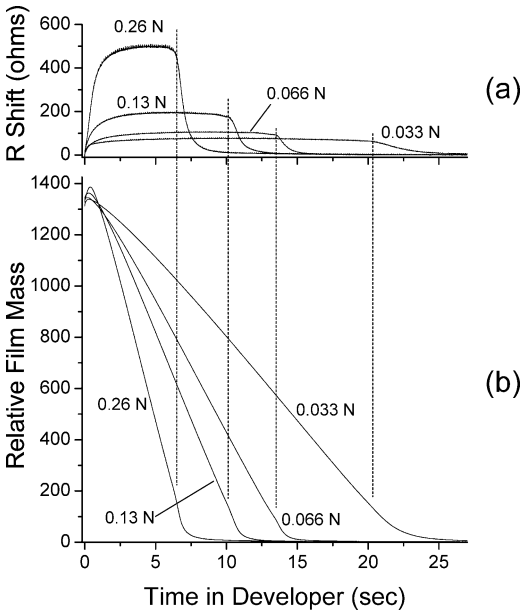

Figure 11. QCM (a) resistance shift and (b) film mass calculated from frequency shifts using the Sauerbrey relation for P(MMA−MAA) dissolving in aqueous alkaline TMAH. The dotted lines indicate the end of the plateau region in the resistance curves, coinciding with an increase in the rate of mass loss.

Visible reflectance measurements performed concurrent with the QCM analyses support this picture. Figure 12 displays reflectance spectra recorded at different points during the dissolution of P(MMA−MAA) in 0.26 N TMAH. The extrema in the spectrum recorded immediately after the alkaline solution contacts the film are at the theoretical limits predicted for a single homogeneous film. With time, both minima and maxima in the measured spectra are displaced from the limiting curves, signaling the formation of an interfacial layer, as depicted in the model calculation of Figure 1c.

Figure 12 also displays calculated spectra from fitting these data to a thin-film optical model where a dry layer and a swollen interfacial layer separated by a sharp front are present. Figure 13a displays the fitted thicknesses of gel and dry layers. By comparing film masses calculated from the reflectance analysis with those calculated using eq I, a interfacial gel layer composition of ~85 vol % liquid is found to be consistent with both data sets. Figure 13b shows the agreement between film masses calculated from the two data sets.

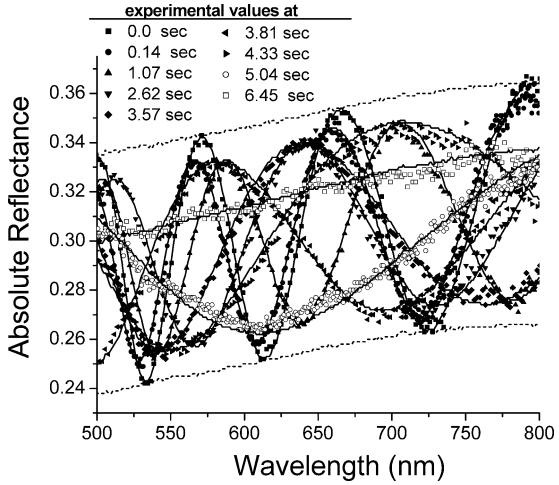

Figure 12. Experimental and calculated visible reflectance spectra during dissolution of P(MMA−MAA) dissolving in 0.26 N aqueous alkaline TMAH. The discrete points are experimental values, solid lines represent best-fit spectra calculated from a thin film optical model, and the dashed lines indicate the theoretical limits for extrema calculated assuming a single homogeneous polymer film with no interfacial layer.

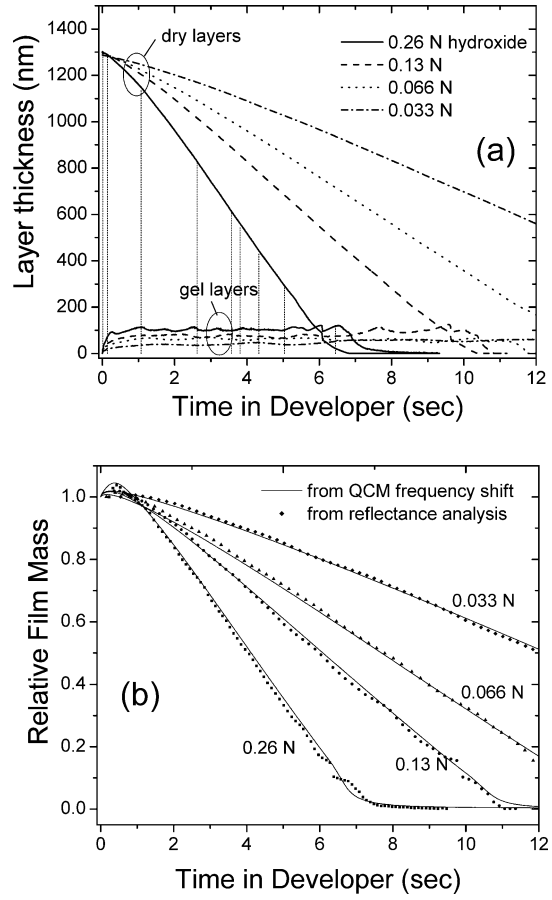

Figure 13. (a) Thickness of gel layer and dry layer for dissolving films of P(MMA−MAA) derived from analysis of visible reflectance data. The vertical dashed lines indicate the positions at which the reflectance spectra in Figure 13 were recorded. (b) Comparison of relative film mass vs time calculated from frequency shifts using eq I and from the visible reflectance analysis.

Initial rates of swelling, derived from initial slope of curves in depicting gel layer thickness vs time, are shown for different TMAH concentrations in Figure 14a. Overall rates of dissolution can be derived in similar

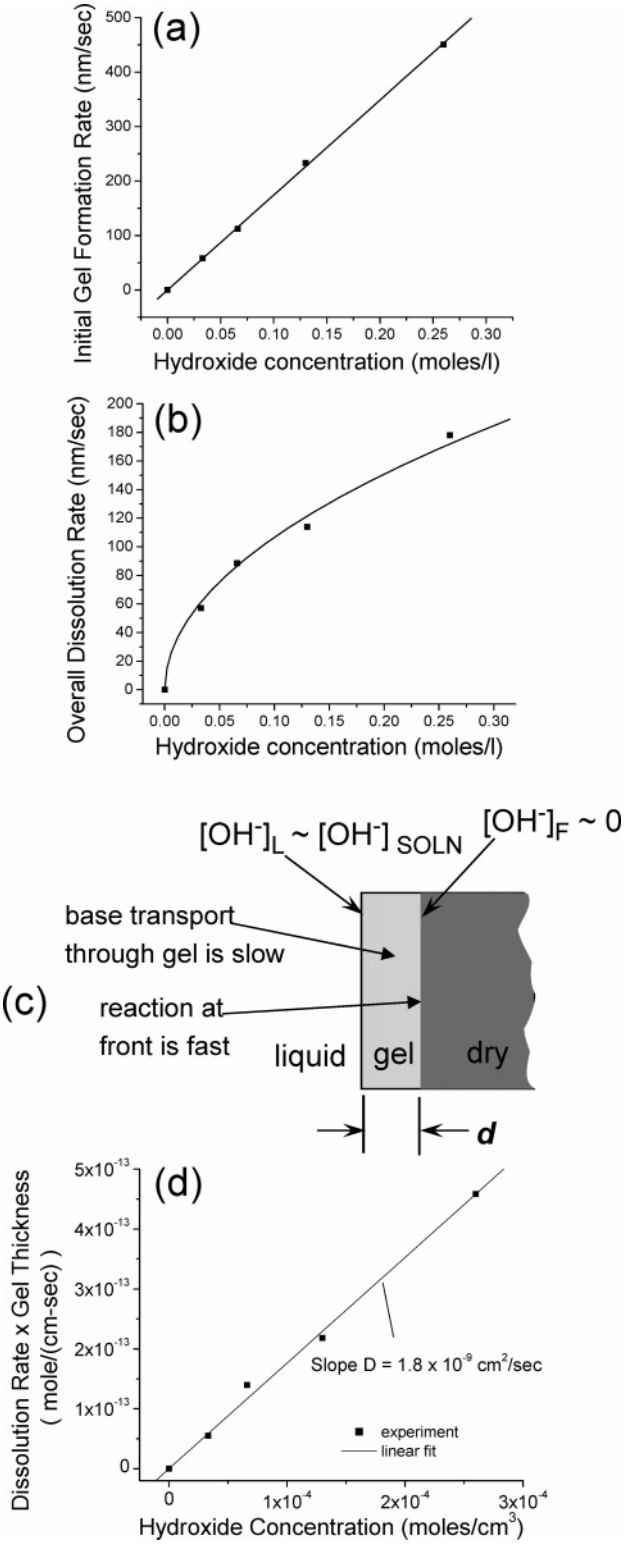

Figure 14. (a) Initial rate of swelling in P(MMA−MAA) as a function of hydroxide concentration. The solid line is a linear fit to the experimental data. (b) Dissolution rate of P(MMA−MAA) as a function of hydroxide concentration. The solid line is a plot of the form rate = $k[OH^-]^{1/2}$. (c) Schematic illustrating the case where base transport through the gel layer is slow compared to the rate of neutralization. (d) Plot of the product of the observed dissolution rate and the gel thickness plotted as a function of solution hydroxide concentration according to eq VII. For this plot the dissolution rates in (b) were converted to mol s^{-1} units using 2.53 mol/L as the concentration of carboxyl groups in the polymer film, a film gravimetric density of 1.23 g/cm^3, and assuming that all carboxyl groups on the polymer chains are ionized upon dissolution.

manner by evaluating the change in the thickness of the dry film layer as a function of time (Figure 14b). Though the initial swelling rate increases linearly with increasing developer concentration, the film dissolution rate increases nonlinearly, roughly in proportion to the square root of $[OH^-]$.

If base transport through the interfacial gel layer is rate limiting, then the schematic drawing in Figure 14c applies. A gradient of hydroxide will exist across the gel layer. The concentration at the liquid−gel interface is approximately that in the bulk solution, and the concentration at the gel−solid interface is ~0 since the neutralization rate is rapid. The hydroxide concentration gradient across the gel layer can therefore be approximated as

$$\nabla \cong ([OH^-]_{soln} - [OH^-]_{front})/d = [OH^-]_{soln}/d \quad (V)$$

where $[OH^-]_{soln}$ and $[OH^-]_{front}$ are the concentrations of hydroxide in the solution and at the gel-dry front, and d is the gel thickness (Figure 14c). The overall rate of dissolution S will then be equal to the diffusion rate of hydroxide through the gel to the advancing front:

$$S = D\nabla = D[OH^-]_{soln}/d \quad (VI)$$

where D is the diffusion coefficient. Rearranging gives

$$Sd = D[OH^-]_{soln} \quad (VII)$$

This states that, if diffusion of hydroxide ion through the gel layer is rate-controlling, then a plot of the product of the observed dissolution rate and gel thickness vs the solution concentration of hydroxide ion should be linear with a slope equal to the diffusion coefficient of hydroxide through the gel layer. Figure 14d shows such a plot, whose linear form supports the supposition that hydroxide ion transport through the gel layer is rate-controlling in this instance. A value for the diffusion coefficient D of 1.8×10^{-9} cm^2/s is calculated by this method. This value is within the range for diffusion of water in poly(ethylene glycol), PMMA, poly(methyl acrylate), poly(dimethylacrylamide), poly(*N*-vinylpyrrolidone), and vinyl ether polymers.[54]

Base-Induced Dissolution of Cresol Novolacs. Arcus first considered the role of interfacial layers in the dissolution of phenolic resins such as novolacs in aqueous base.[18] As evidence to support this, Arcus reported single-wavelength visible interferometry results for interaction of a phenolic polymer with aqueous base. These results (reproduced in Figure 15) were interpreted by Arcus as consistent with formation of a swollen surface gel layer, with three sharp interfaces that produce a complex interferogram with three periodic components.

Recently, an evaluation of Arcus' experiment concluded that the initial section of that trace with three periodicities is not consistent with gel layer formation but instead attributed the pattern to noise in the optical signal, resulting from an air−water boundary disrupted by immersion of the wafer.[56] However, comparison of Arcus' result with interferograms for P(NBCarb-NBCA) swelling (Figure 7) and with those discussed by Durning et al. for PMMA swelling in methanol[4] reveals notable similarities. We have used our four-layer optical model to predict interferograms expected when the phenolic

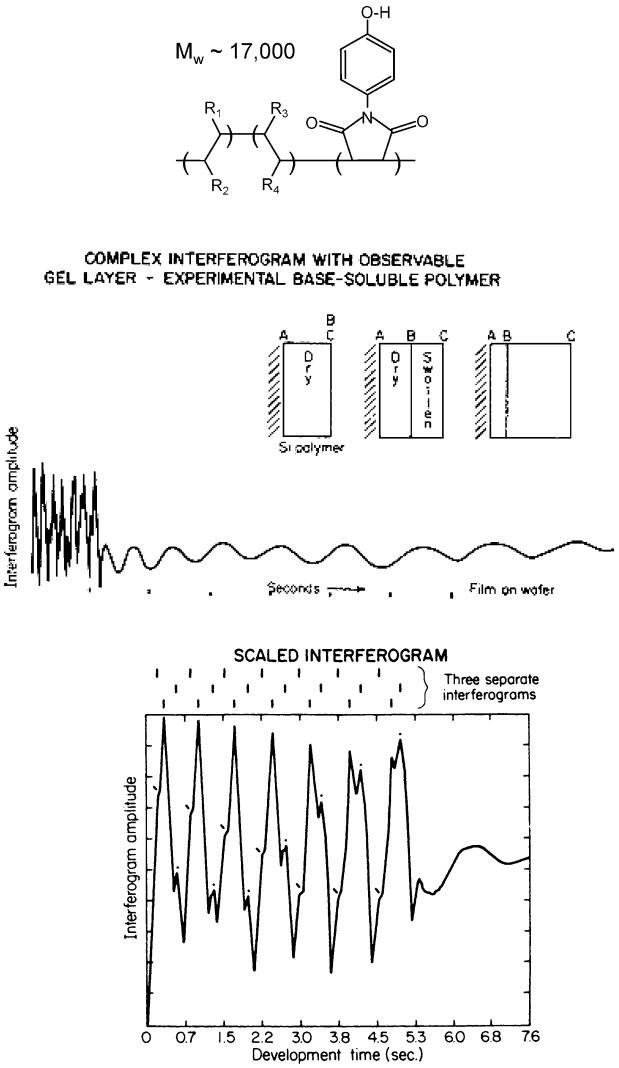

Figure 15. Interferograms at $\lambda = 633$ nm measured during swelling in aqueous hydroxide of the depicted phenolic polymer (reproduced with permission from ref 18). The structure shown here depicts in a general form the composition of the polymer.[57]

polymer of Arcus undergoes two-stage swelling analogous to the P(NBCarb-NBCA) behavior reported here. Our model calculation assumes that Arcus' polymer swells in a manner analogous to the P(NBCarb-NBCA) studied here using the following input: (1) the initial film thickness is ~1325 nm with a refractive index at 633 nm of 1.636;[57] (2) the interferograms in Figure 15 are plotted with reflectance increasing in the downward direction;[57] (3) swelling occurs at such a rate that the dry film thickness decreases at a rate of ~−250 nm/s, the gel thickness increases at ~5× this rate, and the swollen gel layer once formed undergoes a slower secondary swelling at a rate of ~75 nm/s (these rates were selected to scale the time scale of the simulation to the experiment); and (4) the gel composition is ~20 vol % polymer. Curves predicted using these inputs show three series of interdigitated peaks followed by a more conventional single sinusoid after the initial rapid swelling is complete. The detailed fine structures in the calculated interferograms (phase shifts, periods, and relative intensities of the periodic components) are very sensitive functions of the assumed initial film thickness, refractive index, and rates but in all cases reproduce the essential features of Arcus' interferograms of Figure 15. A representative example is shown in Figure 16.

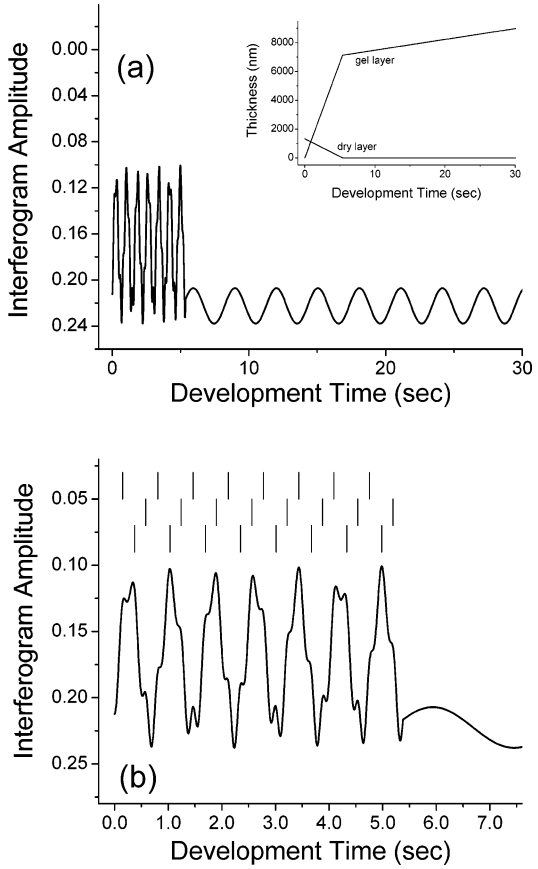

Figure 16. Interferogram at 633 nm calculated for the polymer depicted in Figure 15 with a four-layer optical model, using input parameters listed in the text.

From this we conclude that the interferogram in Arcus' experiment is consistent with gel formation analogous to P(NBCarb-NBCA), supporting his original interpretation and his conclusion that gel layers can be formed in phenolic polymers.

QCM−Visible Reflectance Analysis of Cresol Novolacs. Novolac dissolution behavior is strongly affected by polymer structure, molecular weight, branching, and other factors.[58] The dissolution of two cresol novolac polymers (designated N5, a *m*-cresol novolac, and V6006, a mixture of cresol isomers), with different properties and from different sources, was examined by simultaneous QCM/reflectance analysis. These materials were selected because their dissolution properties typify those of lithographically useful cresol novolacs, and both have been used in practice for the formulation of photoresists based on diazonaphthoquinone dissolution inhibitors. Experimental conditions were chosen so that films of both materials have similar dissolution rates. A detailed examination of their dissolution reveals significant differences in behavior.

N5 Resin. A 1000 nm film of N5 resin dissolves in 0.13 N TMAH solution in ~60 s (Figure 17a). Visible reflectance spectra recorded during dissolution of N5 resin are most simply analyzed using a thin-film optical model that assumes a single polymer layer (that is, no interfacial gel layer is present). No improvement in fit is realized when formation of an interfacial gel layer is introduced into the model. It is useful to pictorially illustrate the agreement between predicted and observed reflectances by comparing plots of the experimental and calculated values at a selection of single wavelengths, each chosen to correspond to maxima and

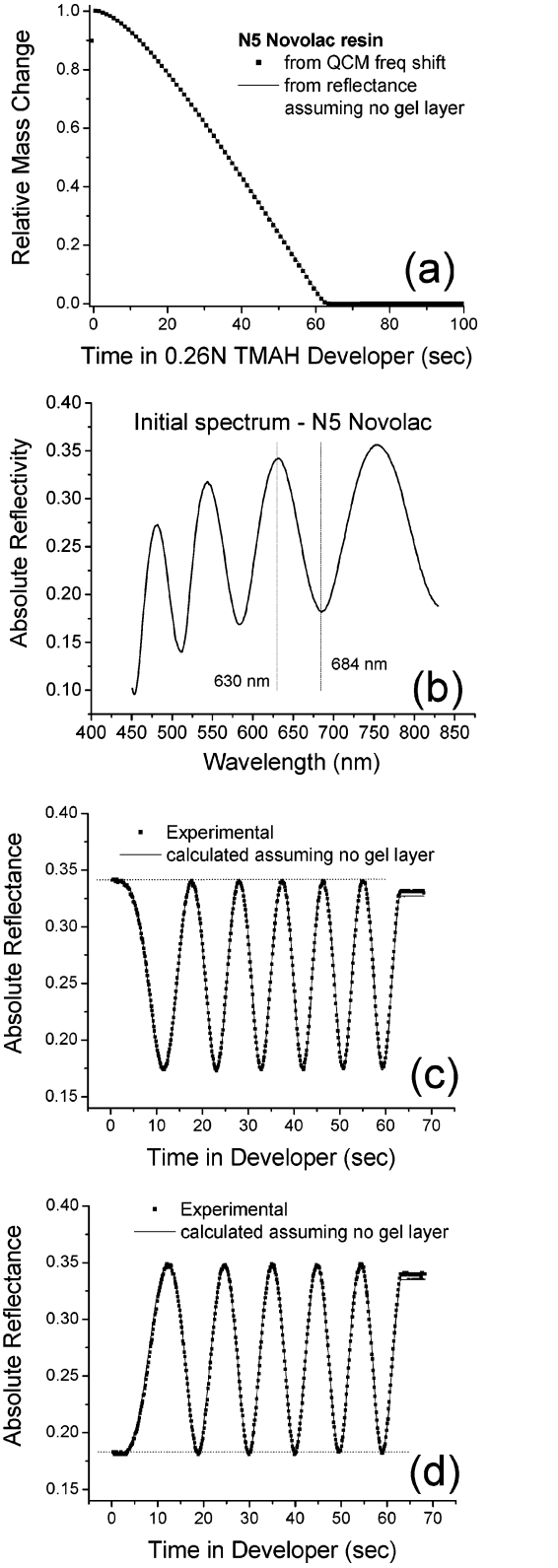

Figure 17. (a) Comparison of film mass vs time calculated from concurrent visible reflectance analysis during dissolution of N5 novolac resin in 0.13 N TMAH with those obtained from Sauerbrey analysis of QCM frequency shifts recorded concurrently. The calculation from the reflectance analysis assumed no gel layer is present. (b) Initial reflectance spectrum of N5 before dissolution, indicating positions of minimum and maximum to be plotted as single-wavelength reflectivities. (c) and (d) display the changes in N5 film reflectance at 630 and 684 nm, respectively, during film dissolution; experimental data are shown as discrete points, and the calculated fit assuming no gel layer is shown as a solid line.

minima in the initial spectrum of the film prior to dissolution (Figure 17b). Such plots for N5 resin are shown in Figure 17c,d. The close agreement between model and experiment is evident. We estimate in this case that this method would not be able to reliably detect formation of a gel layer thinner than ~3 nm so this value serves as an upper limit. The film mass change during dissolution calculated from the optical analysis is plotted in Figure 17a and precisely overlays the QCM data.

For both N5 and V6006 novolac samples, small deviations in the final reflectance at the end of dissolution from that of the bare wafer are noted. This is attributable to the presence of a very thin (10−40 Å) layer of residual base-insoluble material that appears to form on the surface of the chromium-coated QCM crystal. Reflectance analyses of N5 and V6006 films coated on silicon substrates yield results essentially identical in every respect to those on chromium-coated QCM crystals except the post-dissolution offset in reflectance due to the chromium surface interaction is absent. The chromium-coated quartz crystal substrate is necessary so that simultaneous, synchronized QCM and reflectance data can be acquired, thereby avoiding slight run-to-run variations in film thickness and dissolution kinetics that would obscure small differences between the two measurements that are the basis of our analysis.

V6006 Resin. The same experimental analysis of V6006 resin, which exhibits a pronounced initial dissolution induction, yields a different result. Figure 18 displays for V6006 the same curves which Figure 17 shows for N5 novolac, where in both cases the model is restricted to a single film layer and no interfacial gel layer is allowed. In the V6006 instance, though experiment and model are in good agreement at the initial induction stage, they diverge as dissolution begins. The experimental reflectance values at maxima and minima become offset from their theoretical limits in a manner consistent with the formation of an interfacial gel layer. A comparison of mass changes during dissolution calculated from QCM frequency shift and from the optical analysis shows similar mismatch; the single-layer model for reflectance analysis underestimates the film mass. Together these results indicate that the single-layer model does not adequately describe the structure of a dissolving V6006 film.

A second analysis of the V6006 experiment, this time allowing formation of a gel layer in the model, produces a much improved correlation. Figure 19 graphically shows the match between experiment and model for both mass analysis (a) and the single wavelength reflectances (b, c). The calculated thicknesses of the layers are shown in Figure 19d. The improved match between model and experiment is evident. The MSE for fitting calculated and experimental reflectance spectra in this analysis is reduced by a factor of 3.5 compared to the analysis where it was assumed that no gel layer is present. For this material, the gel composition is estimated to be ca. 50 vol % liquid.

Changes in QCM resistance during dissolution can be interpreted as consistent with the formation of a gel layer. The absolute resistance shifts are small, reduced by roughly an order of magnitude or more from those observed with P(NBCarb-NBCA) and P(MMA−MAA). With V6006 the resistance changes during dissolution (shown in Figure 20) can be divided into several regions.

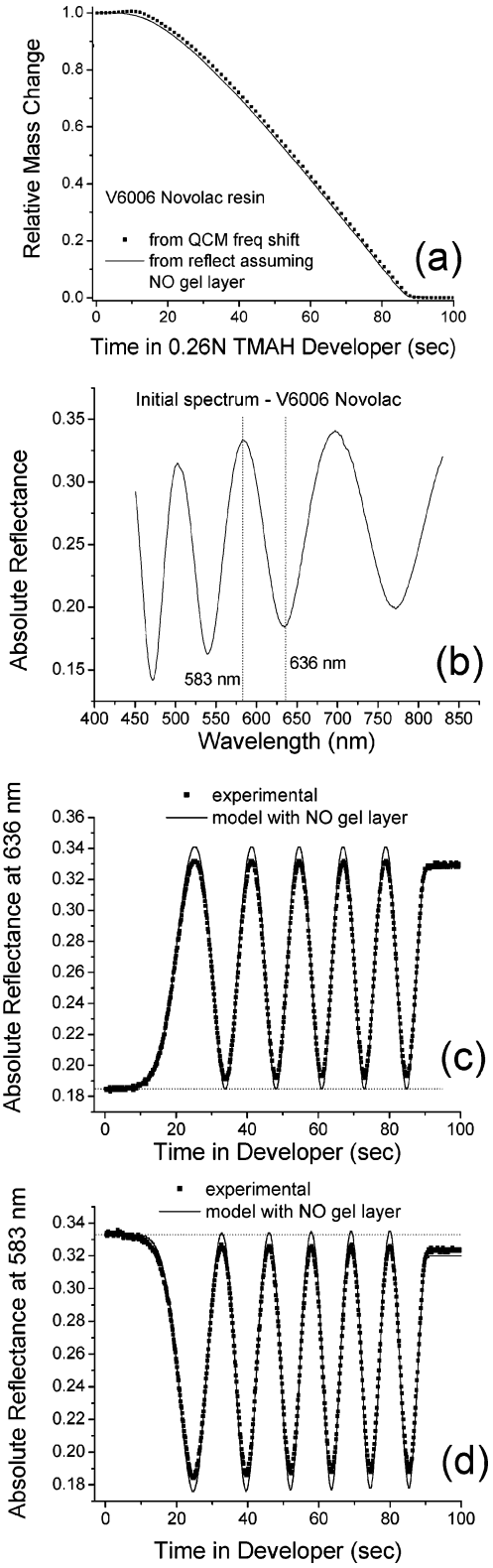

Figure 18. (a) Comparison of film mass vs time calculated from concurrent visible reflectance analysis during dissolution of V6006 novolac resin in 0.26 N TMAH with those obtained from Sauerbrey analysis of QCM frequency shifts recorded concurrently. The calculation from the reflectance analysis assumed no gel layer is present. (b) Initial reflectance spectrum of V6006 before dissolution, indicating positions of minimum and maximum to be plotted as single-wavelength reflectivities. (c) and (d) display the changes in V6006 film reflectance at 636 and 583 nm, respectively, during film dissolution; experimental data are shown as discrete points, and the calculated fit assuming no gel layer is shown as a solid line.

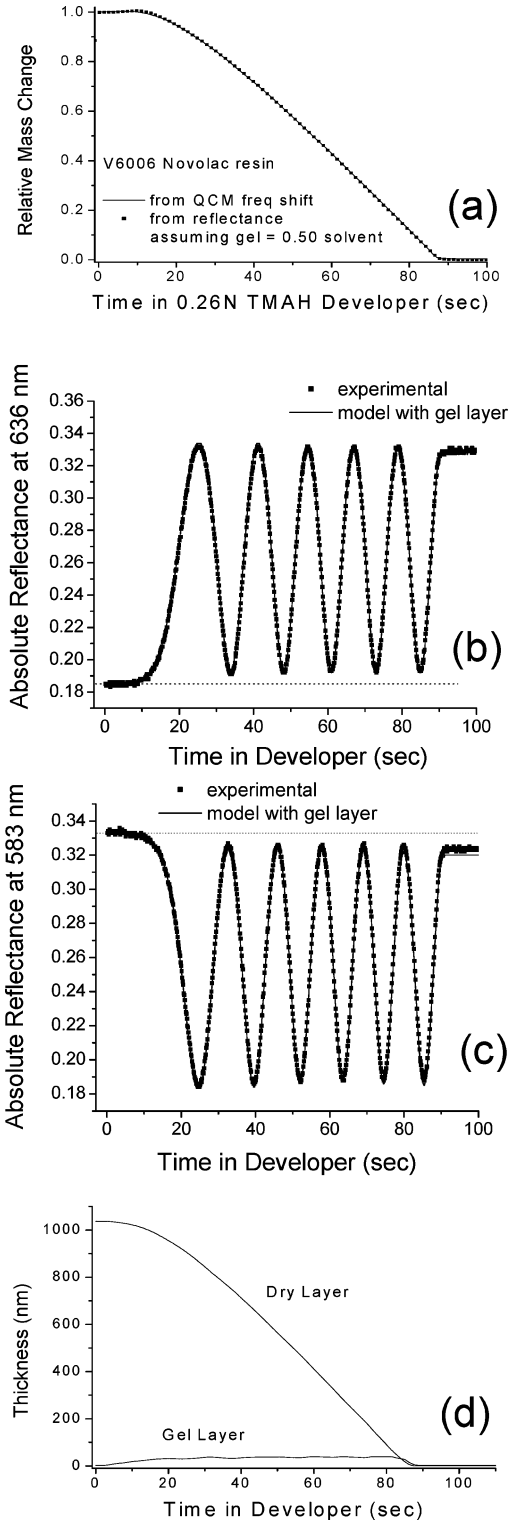

Figure 19. (a) Comparison of film mass vs time calculated from concurrent visible reflectance analysis during dissolution of V6006 novolac resin in 0.26 N TMAH with those obtained from Sauerbrey analysis of QCM frequency shifts recorded concurrently. The calculation from the reflectance analysis allows for the formation of a gel layer. (b) Thicknesses of the dry and swollen films derived from that analysis. (c) and (d) display the changes in V6006 film reflectance at 636 and 583 nm, respectively, during film dissolution; experimental data are shown as discrete points, and the calculated fit when a gel layer is allowed is shown as a solid line.

During the initial induction period resistance increases as the interfacial layer forms. After ~15 s the interfacial layer thickness becomes constant and net dissolution

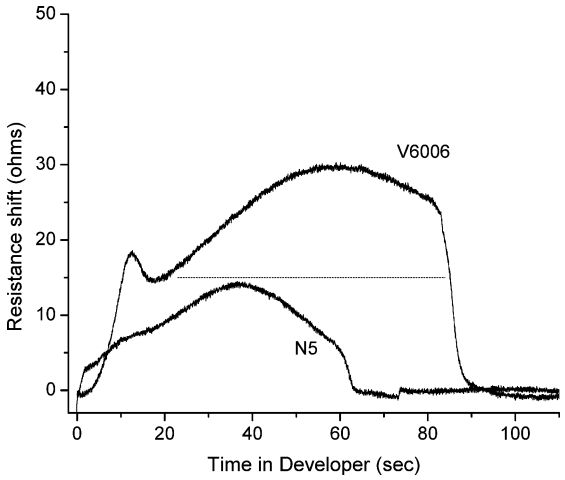

Figure 20. Resistance shifts during dissolution in aqueous TMAH of V6008 and N5 novolac films. The horizontal dashed line is added to guide the eye as to the position of the V6006 plateau region discussed in the text.

begins; at that point the resistance exhibits a slight drop. The resistance shows slowly increasing and then decreasing values as the bulk film dissolves at a constant state, At the point where only gel layer remains, the resistance drops sharply to that of the bare substrate as the gel dissolves.

The resistance behavior of N5 novolac is simpler and appears to be comprised of only the bulk dissolution stage seen in V6006 without the complex early behavior. The N5 resistance shift at the maximum is smaller by a factor of 2, and the overall integrated shift is lower by a factor of 3. We presume that its resistance behavior during bulk dissolution stems from factors unrelated to gel formation. While surface roughness has been shown to influence QCM response in liquids,[59] the reported change in roughness of novolac films during development (increasing from ~0.5 to 2.5 nm)[60] is inconsistent with this being a significant contributor. Possible causes for the observed resistance shift include changes in surface hydrophobicity, or in the structure of the surface-adjacent water layer, as the polymer undergoes ionization and dissolution.[59,61] This effect is seen in both novolac materials. In V6006 this bulk resistance shift appears to superimposed on a plateau analogous to that in P(MMA−MAA) (Figure 11a), atttributable to the gel layer. The "spike" in the resistance shift of V6006 is presumed to be linked to the initiation of dissolution as it appears at the transition from initial swelling to steady-state dissolution.

In recent work by Hunek and Cussler the dissolution of a novolac resin was analyzed using a spinning disk method.[62] They concluded from their kinetic analysis that the dissolution of novolac is best described by a mechanism where both release of ionized polymer from the solid (S3 in their notation) and mass transfer into the liquid phase (S4) are rate-limiting, implying that the two steps have comparable rates. The authors point out that the slow surface release process S3 has been identified in water-soluble polymers such as xanthan and pectin which are known to form swollen gel layers. The authors also note that if S4 is fast, then no intermediate gel layer is formed. We interpret our novolac results as consistent with this description, where the differing behaviors in N5 and V6006 depend on whether S3 or S4 has the larger rate for a given polymer. If the rate of S4 exceeds that of S3, then the

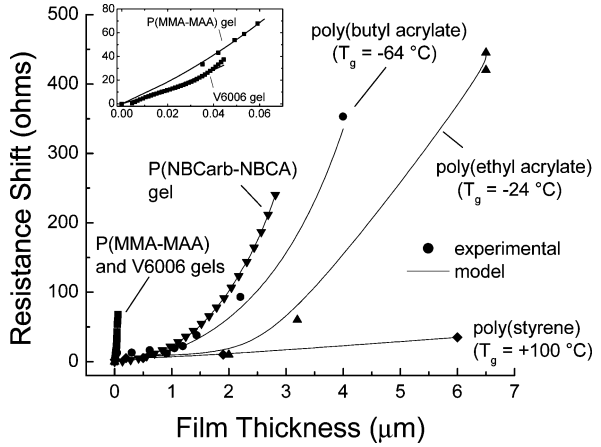

Figure 21. Resistance shifts vs film thickness for a range of polymer films. Discrete points represent experimental data, and lines represent fits using a physical model for a multilayer quartz resonator. The inset shows an expansion of the P(MMA–MAA) gel and V6006 novolac gel data.

Table 1. Values for the Elastic Modulus and Viscosity for Polymer Film Layers Derived by Fitting Experimental Measurements of Resistance vs Film Thickness to the Extended Physical Model for a Coated Quartz Resonator; Properties of Water Are Included for Reference

film	elastic modulus (Pa)	viscosity (Pa s)
poly(styrene)	3×10^9	100
poly(ethyl acrylate)	3×10^8	4
poly(*n*-butyl acrylate)	3×10^7	0.1
P(NBCARB–NBCA) gel	2.3×10^7	0.03
P(MMA–MAA) gel	6.6×10^4	0.0016
Novolac V6006 gel	5.6×10^4	0.0024
thick water layer	0	0.001

N5 behavior results; if the rate of S4 is less than that of S3, then V6006 behavior is observed. The novolac polymer studied by Burns et al.,[56] reported to show no significant gel formation upon dissolution, provides another example of the case where S4 is fast.

An initial dissolution induction is desirable in photoresist dissolution as it leads to a nonlinear response to radiation dose that enhances imaging contrast.[63] The V6006 resin dissolution shows both a pronounced induction period and evidence for a significant gel layer formation, while the N5 material shows much less rate retardation at the initial stage and no detectable gel. This is suggestive that gel layer formation is a factor leading to dissolution induction, at least in this instance, though the potential contributors to dissolution are many, and the relation of dissolution induction in pure polymers to those in more complex resist compositions remains to be established.

Mechanical Properties of Gel Layers. The viscoelastic character of interfacial gel layers can be probed by comparing predictions of a physical model with experimental values for the QCM resistance at different layer thicknesses.[33] Such comparisons are shown in Figure 21 for the three polymers which showed detectable gel layers. Also shown are resistance vs thickness data for films of three reference polymers. The mechanical properties listed in Table 1 were derived by applying chi-square analysis to fit model predictions to experimental data. The gel formed upon swelling of P(NBCarb-NBCA) has roughly the same viscoelastic character as a film of the rubbery material poly(*n*-butyl acrylate), while the gel layers formed during dissolution of P(MMA–MAA) and V6006 novolac have much lower values of both elastic modulus and viscosity.

QCM impedance analysis at 10 MHz has been used by Calvo and co-workers to study the viscoelastic properties of highly hydrated polyelectrolyte gel layers that are analogues to those under investigation here.[64,65] The viscosity values derived from their measurements are within the range we estimate for our three gel-forming polymers. Those authors point out that slow polymer segmental motion in such gels leads to a natural frequency in the 1–10 Hz range and conclude that relaxation of the ionic atmosphere of the polyelectrolyte gel dominates the QCM impedance (resistance) response.[64]

Preliminary Kinetic Modeling. The observed swelling and dissolution behaviors in these experiments are materials-specific, and it would appear difficult to gain insight into any commonality in their behaviors. However, numerical simulations of the dissolution process carried out as part of this work have been successful in this regard and provide information on how the interplay between reaction and diffusion is manifested.

In earlier work[66] we described a kinetics embodiment of the critical ionization (CI) model[46,67] for resist dissolution. In that study, several simplifying assumptions were made: only partially protected homopolymers were treated, gel formation was specified to be minimal, and polymer deprotonation by aqueous base was constrained to occur only in a well-defined thin reaction zone. The simulation methods used here extend that approach and incorporate essential features suited to the materials under study. In the present model the kinetic description has been expanded to support copolymers and terpolymers whose monomer units can have independent ionization kinetics. A deprotonation reaction for a 20-mer terpolymer is written as

$$\mathrm{A}_x\mathrm{B}_y\mathrm{C}_z + \mathrm{OH}^- \underset{k_{\mathrm{rev}}}{\overset{k_{\mathrm{fwd}}}{\rightleftharpoons}} \mathrm{A}_{x-1}\mathrm{B}_y\mathrm{C}_z\mathrm{I} + \mathrm{H}_2\mathrm{O} \quad \text{(VIII)}$$

where $x + y + z = 20$, A and B are neutral ionizable monomers and C is not ionizable, and I is an ionized group. This ionized group is assumed to be surrounded by an aqueous solvation shell. Similar equations can be written for all combinations of A and B ionization steps, leading up to base-induced ionization of all available sites on the polymer molecule. The equilibrium constant $K_{\mathrm{eq}} = k_{\mathrm{fwd}}/k_{\mathrm{rev}}$ is given by the pK_{a} of the ionizable group. To account for the existence of multiple equivalent pathways, statistical factors must be included in the rate expressions. According to the critical ionization model, once the number of ionized sites reaches a minimum value, the entire polymer chain can dissolve. Depending on the initial kinetics, in the course of the simulations a gel layer can be formed in which the average degree of ionization is high enough for the water content to be of the order of 50% or more, as observed experimentally. Individual polymer chains within the gel will of course vary in their degree of ionization and hydration because of the statistical nature of the deprotonation process.

The model was further extended to allow diffusion of aqueous base through the polymer film, treated using conventional Fickian kinetics. Two descriptions were implemented: case I diffusion, where transport is governed by concentration gradients alone and the diffusion coefficient is constant under all conditions, and case II diffusion, where transport depends on local environment as well as concentration gradients and where the diffusion coefficient can vary dramatically

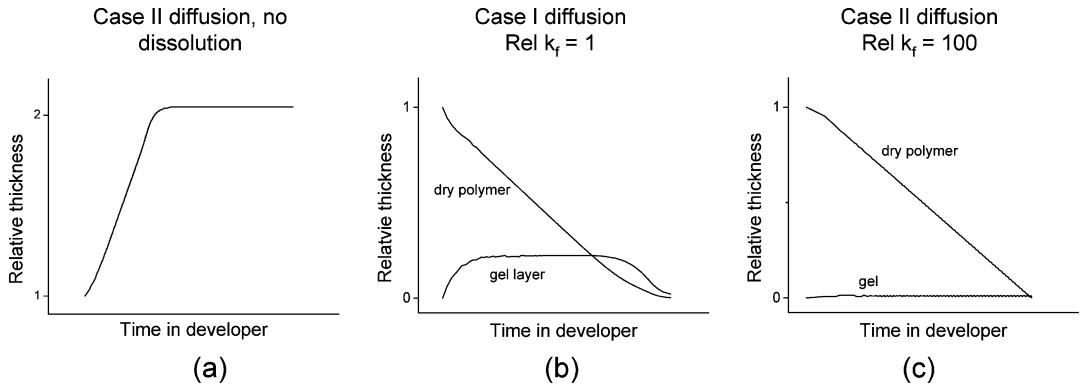

Figure 22. Simulations of polymer swelling and dissolution using three sets of kinetic conditions. These simulations replicate the qualitative behavior observed experimentally in this study. (a) No dissolution path combined with case II diffusion of hydrated base into the polymer film and polymer ionization reaction leads to behavior comparable to P(NBCarb-NBCA). (b) Case I diffusion combined with polymer ionization and dissolution exhibits dissolution behavior comparable to the P(MMA−MAA) polymer. (c) Case II diffusion combined with a more rapid forward polymer ionization rate produces dissolution behavior comparable to V6006 novolac. The noise in the simulated curves results from the stochastic algorithm used.

with location and time depending on the evolution of the system. For case I diffusion the coefficient was chosen to be 1×10^{-8} cm^2/s, a value typical for diffusion of water in polymers[54] and somewhat faster than the value estimated for the P(MMA−MAA) system in this work. Case II diffusion was found to be best described by assuming that the diffusion coefficient increases to a value approximately 100 times greater as ionization proceeds, with simultaneous generation of new free volume in the polymer as it swells and becomes more liquidlike in its character. The simulation code is an internally developed package that has been described previously.[68] Further details of the model will be presented in a separate publication.[69]

As an initial step, we have focused on understanding how variations in diffusion mode and magnitudes of k_{fwd} and k_{rev} affect the experimentally observable dissolution behavior. The reaction rate constants were each varied systematically over 5 orders of magnitude. No attempt was made to fit experimentally observed time scales for a specific system as the focus was on trends as a function of kinetics parameters. The simulation results, which were obtained in the form of concentration vs time curves for all species present in the system, were analyzed to convert them to a form that can be compared directly to experiment by assuming densities for polymer chains in various ionization states.

It was found that the magnitude of the polymer neutralization rate constant k_{rev} had a negligible effect on the kinetics, while that of the polymer ionization rate constant k_{fwd} was directly connected to the characteristics of the gel layer present during dissolution. Because trends and not absolute values of rate constants were the focus in this work, only their relative values are reported. Assumption of case II diffusion was essential for a correct description of the swelling-only system, but the dissolving systems were found to produce behaviors consistent with experiment when either case I or case II transport is assumed.[69] Examples of thickness vs time curves that most closely resemble the behaviors observed in the present work are shown in Figure 22: simple swelling (no dissolution, case II diffusion), dissolution with a thick gel layer (relative $k_{fwd} = 1$, case I diffusion), and dissolution with a thin gel layer (relative $k_{fwd} = 100$, case II diffusion).

It is evident from the simulation results that the most important materials characteristics influencing swelling and dissolution behavior are the intrinsic reactivity of the ionizable group and the response of the mechanical properties of the polymer, which determine the ability of small molecules to move through it, to incorporation of water. Experimental observations involving a range of dissimilar polymers can be understood in a unified way by considering these two factors alone.[69]

Summary and Conclusion

The combination of QCM analysis with reflectance spectrometry can provide significant detail about the structure and composition of polymer films during dissolution. We have applied these methods to probe mechanistic details of the reactive dissolution and swelling of lithographic polymers. With some polymer films, contact with aqueous base leads to the formation of a well-defined gel layer at the liquid−film interface as the film undergoes swelling or dissolution. Analysis of such materials has provided examples where the overall kinetics are controlled by the rate of base transport though the gel layer or by the rate of the chemical reaction within the advancing front. With other polymer structures, dissolution can be characterized as a surface-limited etching reaction with an interfacial layer below our limit of detection. Initial modeling using a kinetic extension of the critical ionization model has captured this wide range of behavior by varying relative rates of the fundamental steps that comprise the dissolution process.

Acknowledgment. This work was supported in part by NSF Materials Science and Research Center Grant 980677 to the Center for Polymer interfaces and Macromolecular Assemblies at Stanford University. The authors thank C. Lamy, G. Le Roy, and M. Navarre of IBM for the V6006 molecular weight characterization and J. Hoffnagle of IBM for guidance in implementing chi-square analysis algorithms.

References and Notes

(1) Thomas, N. L.; Windle, A. H. *Polymer* **1982**, *23*, 531−544.
(2) Hui, C. Y.; Wu, K. C.; Lasky, R. C.; Kramer, E. J. *J. Appl. Phys.* **1987**, *61*, 5129−5136.
(3) Rossi, G.; Mazich, K. A. *Phys. Rev. E* **1993**, *48*, 1182−1191.
(4) Durning, C. J.; Hassan, M. M.; Tong, H. H.; Lee, K. W. *Macromolecules* **1995**, *28*, 4234−4248.
(5) Stamatialis, D. F.; Sanopoulo, M.; Petropoulos, J. H. *Macromolecules* **2002**, *35*, 1021−1027.

(6) Ueberreitter, K. In *Diffusion in Polymers*; Crank, J., Park, G., Eds.; Academic Press: New York, 1968; Chapter 7, pp 219−257.
(7) Ouano, A. C.; Crothers, J. A. *Polym. Eng. Sci.* **1980***, 20*, 160−166.
(8) Herman, M. F.; Edwards, S. F. *Macromolecules* **1990**, *23*, 3662−3671.
(9) Peppas, N. A.; Wu, J. C.; von Meerwall, E. D. *Macromolecules* **1994**, *27*, 5626−5638.
(10) Narasimhan, B.; Peppas, N. A. *Adv. Polym. Sci.* **1997***, 128*, 161−207.
(11) Brannon-Peppas, L. *Med. Plastics Biomater.* **1997**, *4*, 24−44.
(12) Hinsberg, W.; Wallraff, G.; Allen, R. In *Kirk-Othmer Encyclopedia of Chemical Technology*, 4th ed.; Kroschwitz, J., Ed.; John Wiley and Sons: New York, 1998; Supplement, pp 234−280.
(13) Meyerhofer, D. *IEEE Trans. Electron Devices* **1980**, *ED-27*, 921−926.
(14) Hinsberg, W.; Gutierrez, M. *Proc. Soc. Photo-Opt. Instrum. Eng.* **1984**, *469*, 57−64.
(15) Barclay, G.; Hawker, C.; Ito, H.; Orellana, A.; Malenfant, P.; Sinta, R. *Proc. Soc. Photo-Opt. Instrum. Eng.* **1996**, *2724*, 249−260. Ito, H. *Macromolecules* **1998**, *31*, 1024−1031.
(16) Henderson, C.; Tsiartis, P.; Simpson, L.; Clayton, K.; Pancholi, S.; Pawloski, A.; Willson, C. G. *Proc. Soc. Photo-Opt. Instrum. Eng.* **1996**, *2724*, 481−490.
(17) Yeh, T.; Shi, H.; Reiser, A. *Macromolecules* **1992**, *25*, 5345−5352.
(18) Arcus, R. *Proc. Soc. Photo-Opt. Instrum. Eng.* **1986***, 631*, 124−131.
(19) Long, T.; Rodriguez, F. *Proc. Soc. Photo-Opt. Instrum. Eng.* **1991***, 1466*, 188−198.
(20) Choi, S.-J.; Cho, J.-Y. *Proc. Soc. Photo-Opt. Instrum. Eng.* **2001***, 4345*, 952−962.
(21) Allen, R.; Wallraff, G.; Hofer, D.; Kunz, R. *IBM J. Res Dev.* **1997**, *41*, 95−104.
(22) Ito, H.; Wallraff, G.; Fender, N.; Brock, P.; Hinsberg, W.; Mahorowala, A.; Larson, C.; Truong, H.; Breyta, G.; Allen, R. *J. Vac. Sci. Technol. B* **2001***, 19*, 2678−2684.
(23) Hinsberg, W.; Willson, G.; Kanazawa, K. *J. Electrochem. Soc.* **1986***, 133*, 1448−1451.
(24) Toriumi, M.; Ohfuji, T.; Endo, M.; Morimoto, H. *J. Photopolym. Sci. Techn. Jpn.* **1999**, *12*, 545−551.
(25) Ito, H.; Allen, R.; Opitz, J.; Wallow, T.; Truong, H.; Hofer, D.; Varanasi, P.; Jordhamo, G.; Jayaraman, S.; Vicari, R. *Proc. Soc. Photo-Opt. Instrum. Eng.* **2000**, *3999*, 2−12.
(26) Sauerbrey, G. *Z. Phys.* **1959***, 155*, 206−222.
(27) Hinsberg, W.; Kanazawa, K. *Rev. Sci. Instrum.* **1989**, *60*, 489−492.
(28) Kanazawa, K. *Faraday Discuss.* **1997**, *107*, 77−90.
(29) Etchenique, R.; Weisz, A. *J. Appl. Phys.* **1999**, *86*, 1994−2000.
(30) Martin, S.; Bandley, H.; Cernosek, R.; Hillman, A.; Brown, M. *Anal. Chem.* **2000**, *72*, 141−149.
(31) Buttry, D.; Ward, M. *Chem. Rev.* **1992***, 96*, 1355−1379.
(32) Nwank, E.; Durning, C. *Rev. Sci. Instrum.* **1998**, *69*, 2375−2384.
(33) Lee, S.; Hinsberg, W.; Kanazawa, K. *Anal. Chem.* **2002**, *74*, 125−131.
(34) Brown, C.; Horne, D.; Frank, J.; Kanazawa, K. *Proc. 194th Mtg. Electrochem. Soc.* **1998**, 1. Minami, Y.; Kanazawa, K. K. *Proc. Int. Conf. Adv. Polym. Process.* **2001***,* 100.
(35) Herman, I. In *Optical Diagnostics for Thin Film Processing*; Academic Press: New York, 1996.
(36) Berning, J.; Berning, P. *J. Opt. Soc. Am.* **1960***, 50*, 813−815.
(37) Konnerth, K.; Dill, F. *IEEE Trans. Electron. Dev.* **1975**, *ED-22*, 452−456.
(38) Lauchlan, L.; Sautter, K.; Batchelder, T.; Irwin, J. *Proc. Soc. Photo-Opt. Instrum. Eng.* **1985**, *539*, 227−233.
(39) Nivaggioli, T.; Winnik, M. *Chem. Mater.* **1993**, *5*, 658−660.
(40) Reinhardt, M.; Pfeiffer, K.; Lorkowski, H.-J. *J. Appl. Polym. Sci.* **1994**, *51*, 297−301.
(41) Ito, H.; Dalby, C.; Pomerantz, A.; Sherwood, M.; Sato, R.; Sooriyakumaran, R.; Guy, K.; Breyta, G. *Macromolecules* **2000**, *33*, 5080−5089.
(42) Press, W.; Teukolsky, S.; Vettering, W.; Flannery, B. In *Numerical Recipes in C,* 2nd ed.; Cambridge University Press: Cambridge, 1992; Chapter 15.
(43) Willard, H.; Merritt, L.; Dean, J. In *Instrumental Methods of Analysis*; Van Nostrand and Co.: New York, 1974; p 165.
(44) Nakamura, K.; Hatakeyama, T.; Hatakeyama, H. *Polymer* **1981**, *22*, 473−476.
(45) Goldfarb, D. L.; Lin, Q.; Angelopoulos, M.; Soles, C.; Lin, E. K.; Wu, W. *Proc. Soc. Photo-Opt. Instrum. Eng.* **2001**, *4345*, 335−343.
(46) Flanagin, L.; McAdams, C.; Hinsberg, W.; Sanchez, I.; Willson, C. G. *Macromolecules* **1999**, *32*, 5337−5343.
(47) Lehar, O. P.; Spak, M.; Meyer, S.; Dammel, R. R.; Brodsky, C.; Willson, C. G. *Proc. Soc. Photo-Opt. Instrum. Eng.* **2001**, *4345*, 364−474.
(48) Shibayama, Y.; Saito, M. *Jpn. J. Appl. Phys.* **1990**, *29*, 2152−2155.
(49) Hui, C.; Wu, K.; Lasky, R.; Kramer, E. *J. Appl. Phys.* **1987***, 61*, 5137−5149.
(50) Thomas, N.; Windle, A. *Polymer* **1982**, *23*, 529−542.
(51) Tong, H.; Saenger, K.; Durning, C. *J. Polym. Sci., Part B: Polym Phys.* **1989**, *27*, 689−708.
(52) Dolphin, D.; Wick, A. In *Tabulation of Infrared Spectral Data*; Wiley-Interscience: New York, 1977.
(53) Guillet, J. In *Polymer Photophysics and Photochemistry*; Cambridge University Press: New York, 1985; Chapter 3.
(54) Ichikawa, K.; Mori, T.; Kitano, H.; Fukuda, M.; Mochizuki, A.; Tanaka, M. *J. Polym. Sci., Part B: Polym. Phys.* **2001**, *39*, 2175−2182.
(55) Limm, W.; Stanton, D.; Dimnik, G.; Winnik, M.; Smith, B. *J. Appl. Polym. Sci.* **1988**, *35*, 2099−2116.
(56) Burns, S.; Schmid, G.; Trinque, B.; Willson, J.; Wunderlich, J.; Tsiartis, P.; Tayler, J.; Burns, R.; Willson, C. G. *Proc. Soc. Photo-Opt. Instrum. Eng.* **2003***, 5039*, 1063−1075.
(57) Arcus, R. Eastman Kodak, personal communication. The polymer used in Arcus' original study is described as a terpolymer structurally similar to the copolymer IIb in Table 1 of: Turner, S. R.; Arcus, R. A.; Houle, C. G.; Schleigh, W. R. *Polym. Eng. Sci.* **1986**, *26,* 1096−1100.
(58) Dammel, R. In *Diazonaphthoquinone-Based Resists; Tutorial Texts in Optical Engineering;* SPIE Optical Engineering Press: Bellingham, WA, 1993; Vol. TT 11.
(59) Martin, S.; Frye, G.; Ricco, A.; Senturia, S. *Anal. Chem.* **1993**, *65*, 2910−2922.
(60) Burns, S.; Gardiner, A.; Krukonis, V.; Wetmore, P.; Lutkenhaus, J.; Schmid, G.; Flanigan, L.; Willson, C. G. *Proc. Soc. Photo-Opt. Instrum. Eng.* **2001***, 4345*, 37−49.
(61) Duncan-Hewitt, W.; Thompson, M. *Anal. Chem.* **1992***, 64*, 94−105.
(62) Hunek, B.; Cussler, E. *Am. Inst. Chem. Eng. J.* **2002**, *48*, 661−672.
(63) See: Gardiner, A. Ph.D. Thesis, Department of Chemical Engineering, University of Texas, Austin, TX, 1999; Chapter 1 for a review of induction effects in photoresist dissolution.
(64) Etchenique, R. A.; Calvo, E. J. *Anal. Chem.* **1997**, *69*, 4833−4841.
(65) Calvo, E. J.; Etchenique, R.; Bartlett, P. N.; Singhal, K.; Santamaria, C. *Faraday Discuss.* **1997**, *107*, 141−157.
(66) Houle, F.; Hinsberg, W.; Sanchez, M. *Macromolecules* **2002**, *35,* 8591−8600.
(67) Tsiartis, P.; Henderson, C.; Flanagin, L.; Hinsberg, W.; Sanchez, I.; Bonnecaze, R.; Willson, C. G. *Macromolecules* **1997**, *30*, 4656−4664.
(68) Houle, F.; Hinsberg, W.; Morrison, M.; Wallraff, G.; Larson, C.; Sanchez, M.; Hoffnagle*,* J. *J. Vac. Sci. Technol. B* **2000**, *18*, 1874−1885.
(69) Houle, F.; Hinsberg, W., unpublished results. Further details are available on request.

MA048772T